AD-A193 675

RADC-TR-87-135
In-House Report
July 1987

A NOVEL METHOD TO CORRECT RADIATION PATTERN DISTORTION OF CONFORMAL ANTENNAS

John D. Antonucci and Peter R. Franchi

DTIC
ELECTE
APR 2 8 1988

H

ROME AIR DEVELOPMENT CENTER
Air Force Systems Command
Griffiss Air Force Base, NY 13441-5700

88 4 28 039

This report has been reviewed by the RADC Public Affairs Office (PA) and is releasable to the National Technical Information Service (NTIS). At NTIS it will be releasable to the general public, including foreign nations.

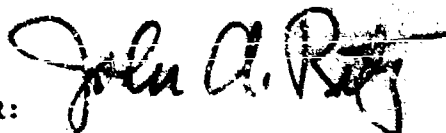RADC-TR-87-139 has been reviewed and is approved for publication.

APPROVED:

JOHN K. SCHINDLER
Chief, Antennas & Components Division
Directorate of Electromagnetics

APPROVED:

ALLAN C. SCHELL
Director of Electromagnetics

FOR THE COMMANDER:

JOHN A. RITZ
Directorate of Plans & Programs

If your address has changed or if you wish to be removed from the RADC mailing list, or if the addressee is no longer employed by your organization, please notify RADC (EEAS) Hanscom AFB MA 01731-5000. This will assist us in maintaining a current mailing list.

Do not return copies of this report unless contractual obligations or notices on a specific document require that it be returned.

REPORT DOCUMENTATION PAGE

1a. REPORT SECURITY CLASSIFICATION	1b. RESTRICTIVE MARKINGS
Unclassified	

2a. SECURITY CLASSIFICATION AUTHORITY	3. DISTRIBUTION / AVAILABILITY OF REPORT
	Approved for public release;
2b. DECLASSIFICATION / DOWNGRADING SCHEDULE	Distribution unlimited.

4. PERFORMING ORGANIZATION REPORT NUMBER(S)	5. MONITORING ORGANIZATION REPORT NUMBER(S)
RADC-TR-87-139	

6a. NAME OF PERFORMING ORGANIZATION	6b. OFFICE SYMBOL (If applicable)	7a. NAME OF MONITORING ORGANIZATION
Rome Air Development Center	EEAS	

6c. ADDRESS (City, State, and ZIP Code)	7b. ADDRESS (City, State, and ZIP Code)
Hanscom AFB Massachusetts 01731-5000	

8a. NAME OF FUNDING / SPONSORING ORGANIZATION	8b. OFFICE SYMBOL (If applicable)	9. PROCUREMENT INSTRUMENT IDENTIFICATION NUMBER
Rome Air Development Center	EEAS	N/A

8c. ADDRESS (City, State, and ZIP Code)	10. SOURCE OF FUNDING NUMBERS			
	PROGRAM ELEMENT NO.	PROJECT NO.	TASK NO.	WORK UNIT ACCESSION NO.
Hanscom AFB Massachusetts 01731-5000	62702F	4600	15	07

11. TITLE (Include Security Classification)

A Novel Method to Correct Radiation Pattern Distortion of Conformal Antennas

12. PERSONAL AUTHOR(S) John D. Antonucci and Peter R. Franchi

13a. TYPE OF REPORT	13b. TIME COVERED	14. DATE OF REPORT (Year, Month, Day)	15. PAGE COUNT
In-House	FROM___ TO___	1987 July	54

16. SUPPLEMENTARY NOTATION

17.	COSATI CODES		18. SUBJECT TERMS (Continue on reverse if necessary and identify by block number)
FIELD	GROUP	SUB-GROUP	Curved phased array Correction technique
09	05		Pattern distortion
17	09		Variable power divider

19. ABSTRACT (Continue on reverse if necessary and identify by block number)

The radiation pattern of a curved phased array antenna is distorted when the beam is scanned. This is primarily due to the change of the appearance of the amplitude taper across the aperture which is a consequence of curvature. The approach described in this report, to correct for this phenomenon, is to adjust the aperture taper as a whole, rather than to adjust each individual radiating element separately. If an anti-symmetric taper is added in the proper proportion to a symmetric taper the original taper can be largely recovered. Typically the sum and difference aperture illuminations of an antenna can provide the needed symmetric and anti-symmetric functions. A relatively simple and practical technique of using the sum and difference networks in combination to correct for curvature effects is demonstrated. This technique uses a variable power divider to distribute the power in a prescribed proportion at an arbitrary scan angle to the sum and difference channels. The optimum amount of signal to be distributed to achieve the maximum restoration is found as a function of scan angle and curvature. ____(Contd)

20. DISTRIBUTION / AVAILABILITY OF ABSTRACT	21. ABSTRACT SECURITY CLASSIFICATION
☐ UNCLASSIFIED/UNLIMITED ☒ SAME AS RPT. ☐ DTIC USERS	Unclassified

22a. NAME OF RESPONSIBLE INDIVIDUAL	22b. TELEPHONE (Include Area Code)	22c. OFFICE SYMBOL
John D. Antonucci	(317) 377-3549	RADC/EEAS

DD FORM 1473, 84 MAR 83 APR edition may be used until exhausted.
All other editions are obsolete.

19.   (Contd)

The analysis is comprehensive, including effects due to the element pattern, antenna size, and the variation of apparent element density. Since attenuators are not used, the method has the added advantage of experiencing no loss of power. The technique can be used to improve any sum and difference illuminations. In this report cosine and sine illumination functions respectively are used.

Contents

iii

Tables

A Novel Method to Correct Radiation Pattern Distortion of Conformal Antennas

1. INTRODUCTION

The development of phased array antennas has, for the most part, been for antennas on planar surfaces. The large phased array antennas, for example, Pave Paws, Aegis, Cobra Dane, and Cobra Judy, are planar arrays. Interest has developed in phased arrays on curved surfaces because of the anticipated need for antennas conformal to aircraft. When scanning, curvature has a detrimental effect on the antenna's radiation pattern; the pattern becomes distorted and the sidelobes are increased. The effect is influenced by factors such as the element pattern, the extent of curvature, and the antenna size, and becomes especially pronounced as the scan angle increases.[1, 2, 3]

1. Wojtowics, J., Ramsey, K.G., and Fontana, T. (1963) Conformal array analysis, Proceedings of the 1983 Antenna Applications Symposium, RADC-TR-84-52, AD A142754, Vol. 2.

2. Herper, J.C., Hessel, A., and Tomasic, B. (1985) Element pattern of an axial dipole in a cylindrical phased array, Part 1: Theory, IEEE Trans., AP-33(No. 3).

3. Ludwig, A.C. (1985) Antenna Curvature Analysis, RADC-TR-85-131, AD B097555L.

The purpose of this report is twofold. First, it is to take a first order approach to explain the effects due to curvature and thereby gain insight into the parameters involved. Second, but foremost, the purpose is to demonstrate a relatively simple and practical technique to correct for curvature effects. Correction implies recovering the form of the pattern that is present at broadside. When the beam of a planar array is scanned, the integrity of the pattern is maintained. For this reason, the equivalent planar array is used as a reference or ideal for the curved array to emulate. A straightforward approach to correct the antenna pattern would be to adjust the amplitude and phase of each individual radiating element. This procedure would be unwieldy and highly impractical. Introducing either attenuators or power dividers into the system, in order to control the amplitude of each element, would greatly increase both rf network and controlling network complexity. In addition, cost, errors, failure rate, weight, and space limitation problems would considerably increase. Attenuators would also introduce power loss.

The approach described in this report is to adjust the aperture taper as a whole. We begin by considering the position of the radiating elements on a curved surface projected on to a straight line perpendicular to the propagation path. The element spacings on the line are shortened from those on the curved surface, and become more so at increasing scan angles. This causes the effective array amplitude taper to become altered, and at scan angles other than zero degrees becomes asymmetrical. The changed taper results in antenna pattern distortion. By adding in the proper proportion an anti-symmetric taper to the symmetric taper, the symmetry of the original broadside taper can be largely restored. This correction can be implemented with the sum and difference networks of the conformal phased array antenna that yield, at broadside, symmetric and anti-symmetric functions respectively. The concept described in this report is to restore, as much as possible, the original aperture taper by adding, as a function of scan angle, some of the energy in the difference network to the energy in the sum network. A simple variable power divider is used to distribute the power, in a prescribed proportion, in the sum and difference channels of the antenna network. This scheme does not use attenuators, and, subsequently, there is no loss of power. Also, each element is not adjusted individually, thereby, making the technique practical and easily implemented.

2. EXAMINATION OF FIRST ORDER CURVATURE EFFECTS

2.1 Model of a Conformal Array

The approach in this study is to investigate the effect of curvature on an antenna radiation pattern based on geometrical considerations. Phenomena such as creeping waves and mutual coupling will be neglected. These effects are considered second order and less influential. The physical model that we consider is an array of a fixed number of elements (66 in this case) and a fixed element spacing ($\lambda/2$). The projection of the curved array on to a straight line perpendicular to the beam direction would result in a projected array that is shorter than the original planar array. The radiating elements on the curved surface are positioned differently in three-dimensional space compared to the elements on the planar surface; this difference brings about the distortion of the wavefront from the equivalent plane surface and accounts for the main effect on the radiation pattern. Primarily, this first order effect on the close-in sidelobes will be addressed in this report. Grating lobe effects will not be investigated.

Of the different types of aperture illuminations, only one will be considered in order to demonstrate the effect of curvature and the correction technique. The aperture will have a cosine illumination with each element having a $\cos^{1.5}(\gamma)$ pattern where γ is a general angular variable. This element pattern approximates measured element patterns and is accurate for patch radiators, narrow slots, or dipoles on a cylinder in which the E-field is along the cylindrical axis. Blockage effects are included. The element radiates only up to the line drawn from it through the next succeeding element (very nearly the tangent line). Although a section of a ring array is being investigated, the results apply to the principal plane cut of a section of a cylindrical array formed by the three-dimensional extension of the ring array. There are no cross polarization considerations in our model. The hypothetical case of an isotropic element pattern, used to demonstrate the influence of the element pattern on curvature effects, is addressed in Appendix A.

2.2 Distortion of Wavefront as a Function of Scan Angle

Consider a series of radiating elements equally spaced along a curved line. When the positions of the elements are projected onto a straight line normal to the line of projection the element spacings on the straight line, as previously, mentioned, are shortened from those on the curved surface. The projected spacings are now not uniform, but vary continuously along the array. The change in the spacings are small at broadside, but increase as the angle of projection off of broadside increases. The apparent change in element spacings cause the effective

3

array amplitude taper to become altered. At scan angles other than zero degrees, the taper is skewed; the greater the scan angle, the greater the skewness. The asymmetrical amplitude taper greatly contributes to the antenna pattern distortion. Figure 1 demonstrates a cosine aperture illumination (showing nine elements) which changes at a scan angle θ_o. In the broadside direction, the taper is a slightly distorted but symmetrical projection of a cos ($\pi n/K$) aperture amplitude distribution for the sum pattern, where n is the element number in which the center element is zero and K is the total number of element spacings. At the scan angle, θ_o, the figure shows how the taper becomes skewed due to the displaced positions of the elements along the line of projection. For example, the center element's position is no longer at the center of the projection line. The center element retains the peak amplitude value of the cosine taper, and therefore, the maximum amplitude is shifted off-center. The other elements follow accordingly. In this manner the original taper becomes skewed. Figure 2 depicts the same phenomenon taking place for a sin ($2\pi n/K$) amplitude distribution for the difference pattern. As the scan angle increases, or as S/R, S being the surface length and R being the radius of curvature, increases, the center element is shifted further off-center and the asymmetry increases. This distance off-center serves as an indicator of distortion. The above discussion dealt with the dependence of the field at the aperture due only to excitation coefficients of the elements and not to their individual patterns. However, the element pattern must also be included in order to obtain the total field. Therefore, the general discussion of the field at the aperture would include a multiplying factor, A_e, which is the amplitude of the element pattern and is a function of scan angle.

Figure 3 shows, for an arbitrary scan angle, the position of the elements on the projection plane and the distortion of the amplitude taper as compared to a cosine illumination function in that plane. The center element is at the origin of the x, y coordinate system, and the other elements are numbered accordingly. The cosine value of the nth element is cos ($\pi n/K$) where, for convenience, the total number of elements, K + 1, is chosen to be odd. The distance of the nth element along the X axis is found to be given by the following equation:

$$X_n = 2R \sin\left(\frac{ns}{2R}\right) \sin\left(\frac{\pi}{2} - \theta + \frac{ns}{2R}\right) \tag{1}$$

where R is the radius of curvature, θ is the scan angle, and s is the surface length between two consecutive elements. A plot of X_n vs the cos ($\pi n/K$) illumination (the peak amplitude being normalized to one) reveals the kind of distortion depicted in Figure 3. The same type of distortion holds for the difference function that is given by sin ($2\pi n/K$), shown in Figure 4. The cosine curve in the projection plane is shown in the X', Y' coordinate system. The cosine curve here is given by:

4

Figure 1. Cosine Aperture Illumination on a Conformal
Phased Array Antenna. At the scar angle θ_0, the
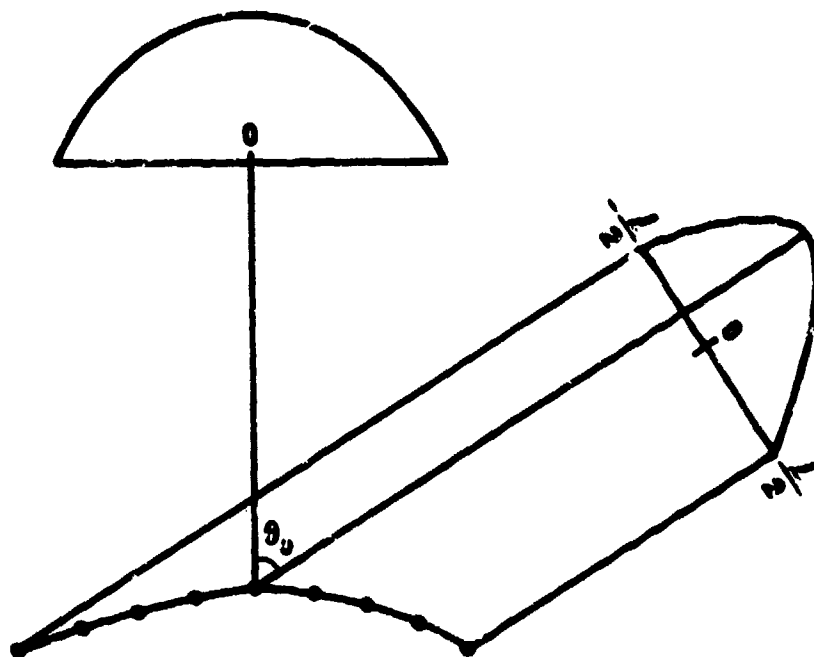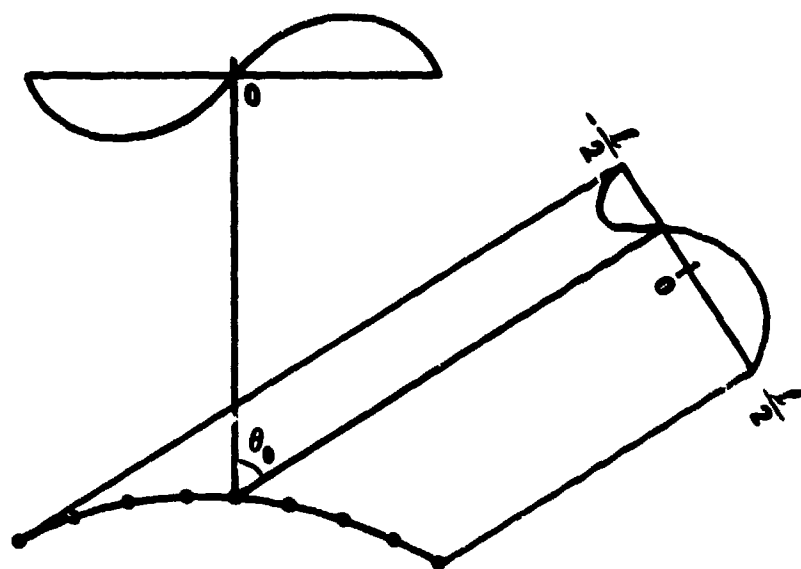illumination becomes skewed

Figure 2. Sine Aperture Illumination on a Conformal
Phased Array Antenna. At the scan angle, θ_0, the
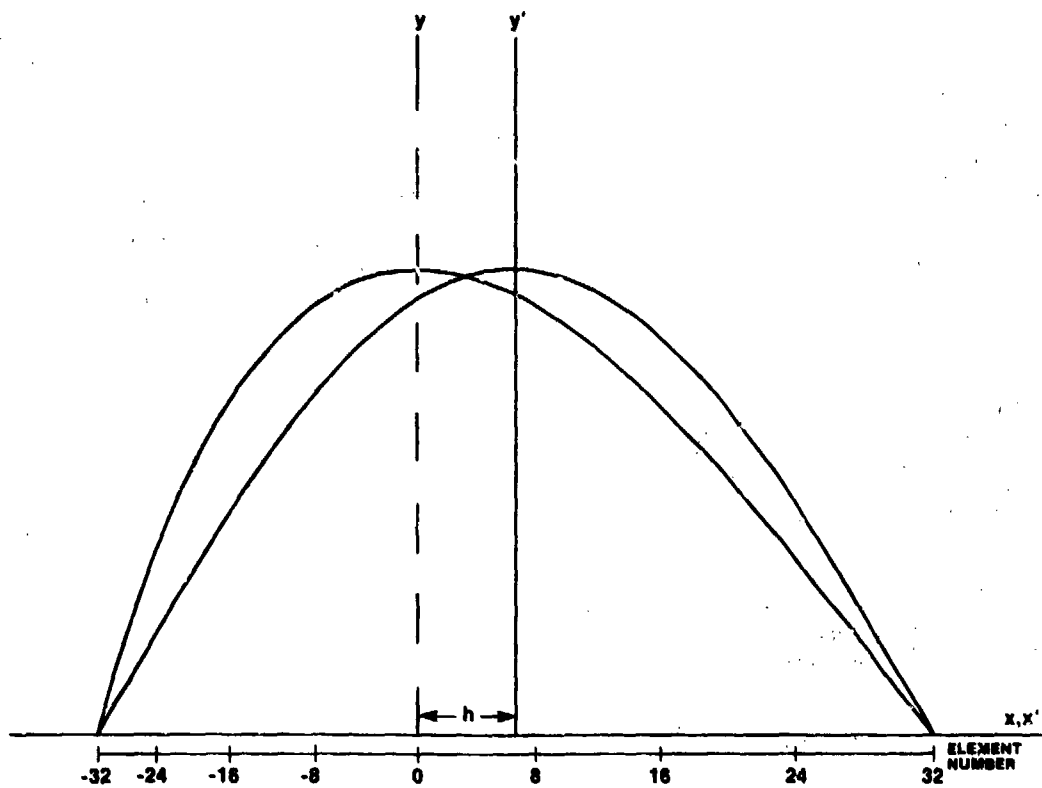illumination becomes skewed

5

Figure 3. Distortion in the Projection Plane of Cosine Amplitude Taper on Curved Surface

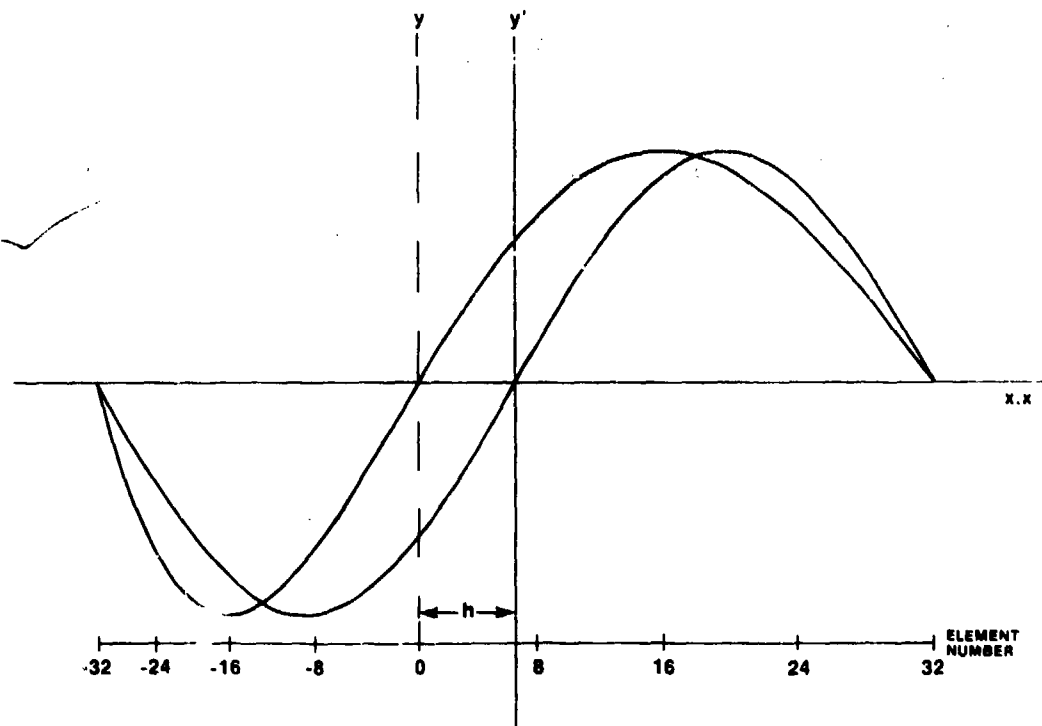Figure 4. Distortion in the Projection Plane of Sin 2γ Amplitude Taper on Curved Surface

6

$$Y' = \cos\left(\frac{\pi X'}{\ell}\right) \tag{2}$$

$$Y' = \cos[\pi(X_n - h)/\ell] \tag{3}$$

where

$$h = R[1 - \cos(Ks/2R)]\sin\theta \tag{4}$$

$$\ell = 2R\sin(Ks/2R)\cos\theta \tag{5}$$

h being the distance the center element shifts off of the geometrical center; ℓ being the length of the array in the projection plane. The difference between the two curves at the nth point, including the effect of the element pattern, is $A_e \cos(\pi n/K) - \cos(\pi X'/\ell)$. This is a measure of the distortion between the two curves.

2.3 Apparent Change of Element Density as a Function of Scan Angle

Thus far, the distortion of the amplitude taper has been considered. However, there is another contributor to the distortion of the radiation pattern. The other factor is the change of the density of the elements when observed in the projection plane. This causes a change in the field density. The elements on one end become "bunched up" causing the local field density to increase. Increasing the element density is equivalent to increasing the field that would otherwise be present if the elements were uniformly spaced. The apparent element density and resulting distortion increases as the scan angle increases. Consider the field of the nth element to be $E(n)$, and contained in a "tube" whose linear cross section is d_n. The length (d_n), extends between the midpoints of the two immediate elements, one on each side of the nth element. If the elements in the projection plane were uniformly spaced, than an element's field would be in a tube whose width was equal to the element spacing. If the nth element's equivalent field is $E'(n)$ and the tube's linear width is D', then

$$E'(n)/D' = E(n)/d_n \tag{6}$$

$$d_n = (X_{n+1} - X_{n-1})/2 \tag{7}$$

$$D' = \ell/K \tag{8}$$

7

where X_{n+1} and X_{n-1} are defined by Eq. (1). $E(n)$ is the amplitude taper in the projection plane. $E'(n)$ represents the effective field when the non-uniform element spacing is made uniform.

$$E'(n) = E(n) F(n) .$$ (9)

$F(n)$ will be referred to as the density function and is given by:

$$F(n) = \frac{2\ell}{K(X_{n+1} - X_{n-1})} .$$ (10)

The effective amplitude taper in the projection plane is $F(n)A_e \cos(\pi n/K)$ plotted as a function of $X(n)$ for the sum pattern, and $F(n)A_e \sin(2\pi n/K)$ plotted as a function of $X(n)$ for the difference pattern. The distortion of the radiation pattern is due to the difference between the shapes of the two curves in the projection plane, and the difference between their element densities. This difference between the two curves at each element is now expressed as $G F(n)A_e \cos(\pi n/K) - \cos(\pi X'/\ell)$ where G is the normalization factor.

3. RESTORATION OF THE COSINE APERTURE TAPER

3.1 Correction Method Applied

As indicated earlier, the $\cos(\gamma)$ curve and the $\sin(2\gamma)$ curve are both distorted in the projection plane. By adding these two functions, the original cosine taper can be approximated in the projected plane. This addition is accomplished by using the sum port and difference port simultaneously. The power is distributed, without loss, by a variable power divider.[4] The idea behind a variable power divider is to split the signal entering in one arm and then, by phase adjustments, control the amount of power going into its two output ports. Each port is part of a network that generates across the array, a $\cos(\gamma)$ and a $\sin(2\gamma)$ distribution respectively. Figure 5 shows the variable power divider in the antenna system. The signal from the sum port, Σ, is distributed between the sum and difference ports, Σ', and Δ', respectively. A portion of the signal in the difference network is added, at the elements, to the signal from the sum network. For the receive mode, the principle of reciprocity applies. The optimum fraction of power to be distributed to each port can be found that achieves a best fit to the $\cos(\gamma)$ taper in the projection plane

4. Rudge, A. W., Milne, K., Olver, A. D., and Knight, P. (1982) The Handbook of Antenna Design, Vol. 1, p. 490, Peter Peregrinus Ltd., London, U. K.

at a particular scan angle. Generally, if A and B are designated the amplitude of the energies in the sum and difference ports respectively, then A and B will be chosen such that A cos (γ) + B sin (2γ) approximates cos (γ'), where γ' is the variable in the projection plane. The best fit would be to obtain the minimum error between the shape of the corrected curve and the undistorted cosine curve. Since we are matching curve shapes, the curves are to be normalized; the corrected curve is to be normalized to one. The difference between the two curves at the nth point is now expressed by:

$$\delta_n = G(B)F(n)A_e [A \cos(\pi n/K) + B \sin(2\pi n/K)] - \cos(\pi X'/\ell) \tag{11}$$

where

$$G(B) = \left[\frac{1}{F(n)A_e [A \cos(\pi n/K) + B \sin(2\pi n/K)]} \right]_{max} . \tag{12}$$
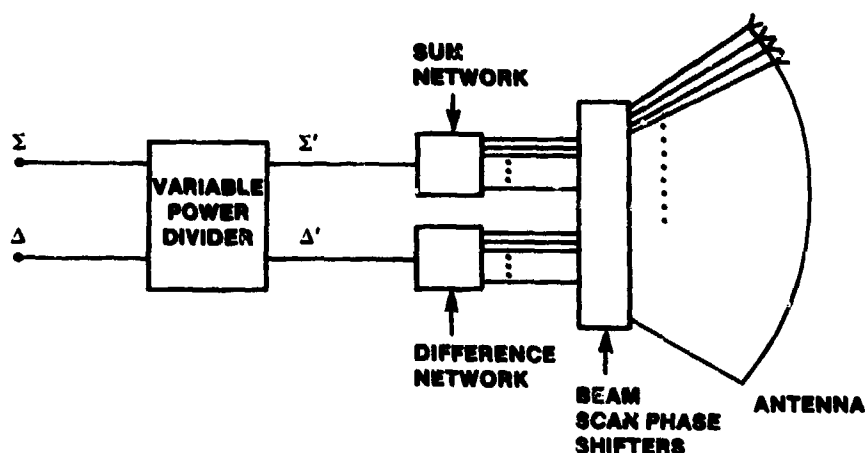

Figure 5. Variable Power Divider Incorporated Into the Antenna System

The constraint in the addition of the two networks is that the total power remains constant. If the input power is normalized to one, then

$$A^2 + B^2 = 1 . \tag{13}$$

Ultimately, the equation used to match the distorted curve to a cosine curve with uniformly spaced elements is the following:

$$\delta_n = G(B)F(n)A_e[\sqrt{1-B^2}\cos(\pi n/K) + B\sin(2\pi n/K)] - \cos[\pi X_n \cdot h)/\ell] .$$

(14)

The total deviation between the two curves is the sum of the δ_n's over all n. Since the absolute value of δ_n is of interest, it is mathematically convenient to use δ_n^2 instead of δ_n. The value to be calculated is the sum of the squares of the deviations, ϵ, that is defined as:

$$\epsilon = \sum_{n=-K/2}^{K/2} \delta_n^2 .$$

(15)

An iterative procedure is used to determine B. First, G is found, when B is equal to zero. Using this value of G, B is solved for which ϵ has a minimum value. Using this value of B a second G is determined, and subsequently a final B, referred to as B_o, is obtained. B_o is quite accurate since there is a rapid convergence. B_o is the fraction of the amplitude from the difference port that yields the minimum value of ϵ, or the best fit of the corrected curve to the cosine curve with uniformly spaced elements.

3.2 Calculated Corrections and Their Associated Errors

The values of B_o as a function of scan angle, θ, with S/R as a parameter, and with A_e equal to $\cos^{0.75}(\theta)$ (a $\cos^{1.5}(\theta)$ power radiation pattern) are shown in Table 1. There were no values chosen in which element blockage was present. Blockage occurs according to the following formula:

$$\theta_B \geq \pi/2 - S/2R + s/2R .$$

(16)

Since, when S/R = 2, (S = 32λ, R = 16λ, s = $\lambda/2$) blockage occurs at 33.6°, the case of S/R = 2 and $\theta = 40°$ was not used. Figure 6 shows how the error, ϵ, varies with scan angle for particular values of S/R. The graph demonstrates the extent to which the error is reduced by introducing the correction. When there is no correction, or B_o equals zero, it is observed that the curve of ϵ vs θ follows approximately a $\tan^2\theta$ curve. This relationship can be deduced from Eqs. (4) and (5). The distortion increases as h increases, h being the distance that the projection of the center element is displaced from the geometrical center of the projected array.

10

More precisely, the factor to be considered is the proportion of the projected array length that the center element is displaced, or h/ℓ. Since ϵ is obtained from the square of the distortion, then:

$$\epsilon \; \alpha \; \left(\frac{h}{\ell}\right)^2 . \tag{17}$$

Using equations for 4 and 5 for h and ℓ respectively, one obtains:

$$\epsilon \; \alpha \; \tan^2\left(\frac{S}{4R}\right) \tan^2(\theta) . \tag{18}$$

Table 1. Correction Factor, B_o, as a Function of Scan Angle, θ_o, and the Curvature Factor, S/R

θ_o	B_o		
	$\frac{S}{R} = 1.07$	$\frac{S}{R} = 1.6$	$\frac{S}{R} = 2$
20°	.105	.169	.227
30°	.165	.264	.351
40°	.236	.376	

This dependency is, to a large degree, verified by the graph in Figure 6. The equation is approximate, but reasonably accurate. It shows the variation of pattern distortion as the scan angle and curvature are changed. The solid curve shows the extent of the uncorrected amplitude taper error, that, in turn, indicates the degree of distortion of the radiation pattern. The dashed curve is the residual error after correction.

In Figure 6, one notices that the degree of error improvement increases as the scan angle increases. Intuitively, one may have expected the opposite to occur. However, adding an anti-symmetric function to a symmetric function does not help to restore symmetry unless the symmetric function is asymmetrical or skewed. At broadside, the symmetric function is not skewed, and, therefore, at broadside, there is no improvement. As the scan angle is increased, both functions become more

11

skewed, and, therefore, there becomes more opportunity for improvement. The
aperture taper could have been matched to the slightly changed broadside taper.
Than a modified cosine taper would have been our reference illumination, and there
would have been no error at broadside. However, in the present study, we chose
not to do this. Figures 7a through 7h show plots of the E-field at the aperture taking
into account aperture taper distortion, apparent change of element density, normali-
zation, and the element pattern. The plots depict the distortion of the amplitude in
the projection plane relative to the cosine curve. The correction curve is also
plotted. The results of the plots are consistent with the conclusions drawn in the
error curves of Figure 6. The improvement of the distorted curve is quite good,
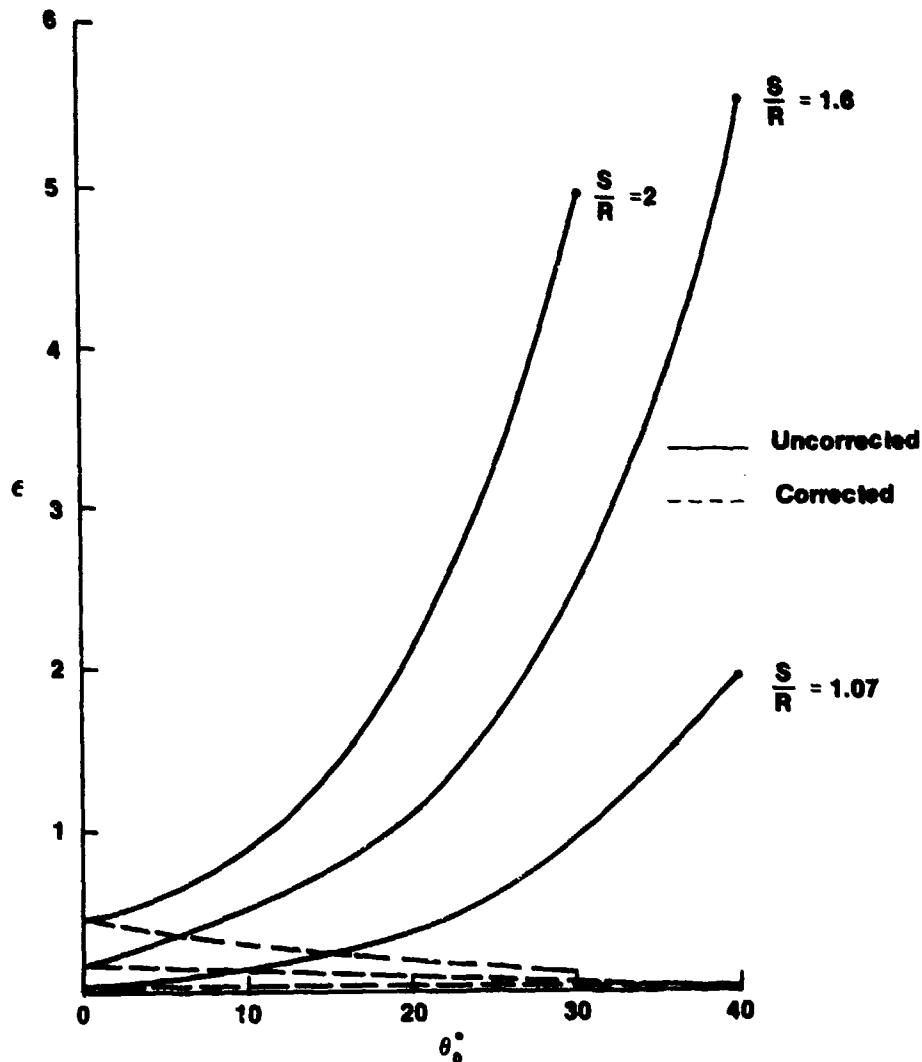especially at the higher scan angles.

Figure 6. Error, ϵ, the Measure of the Difference Between the
Distorted Curve and the Aperture Cosine Curve, is Plotted as a
Function of Scan Angle, θ_o, With Curvature, S/R (the subtended
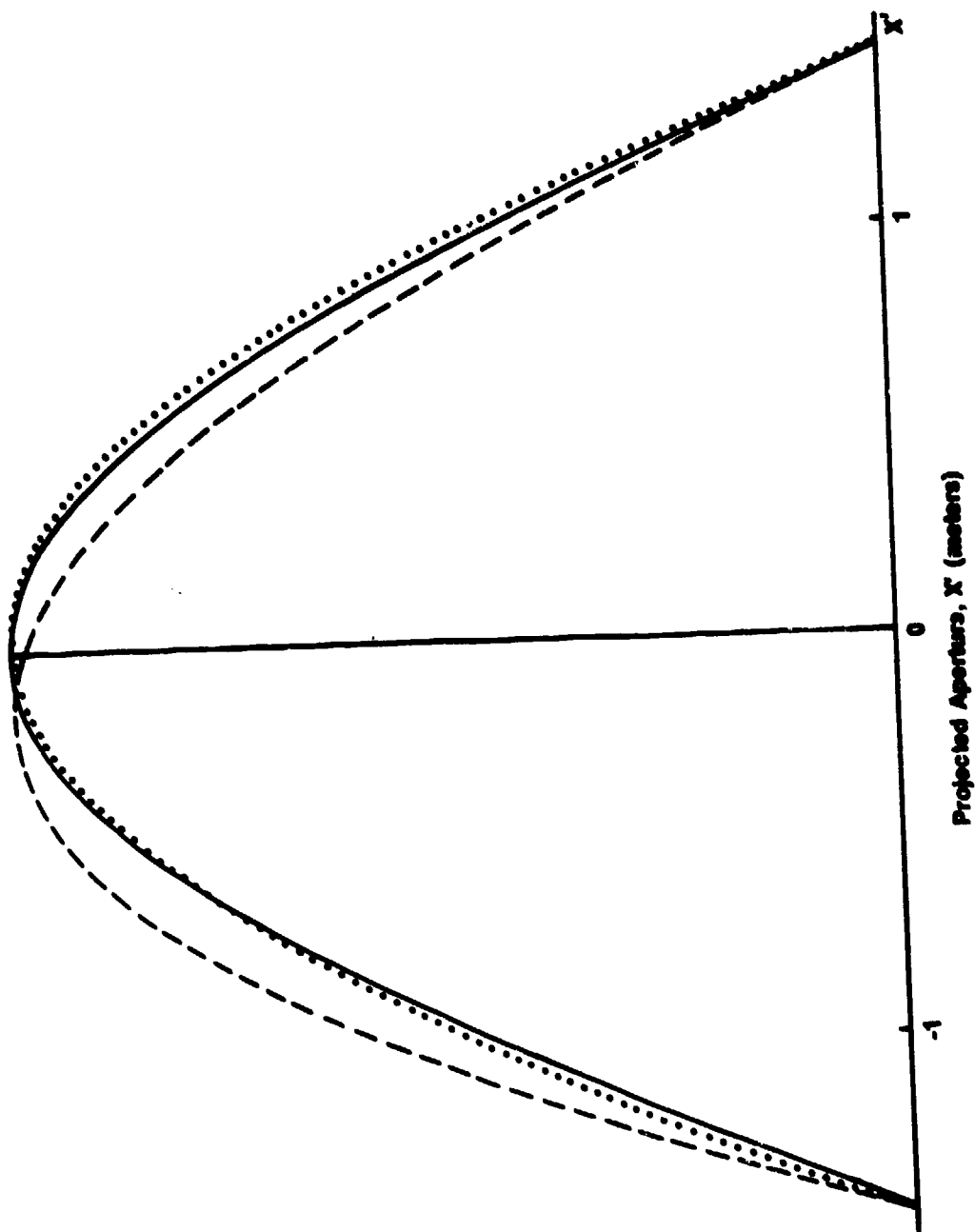angle), as a Parameter

12

Figure 7a. Amplitude at the Aperture in the Projection Plane at Scan Angle, θ_o, and Curvature, S/R. The solid line is for the ideal cosine (planar array); the dashed line is for the distorted (curved array); and the dotted line is for the curved array with the correction. $\theta_o = 20°$, S/R = 1.07

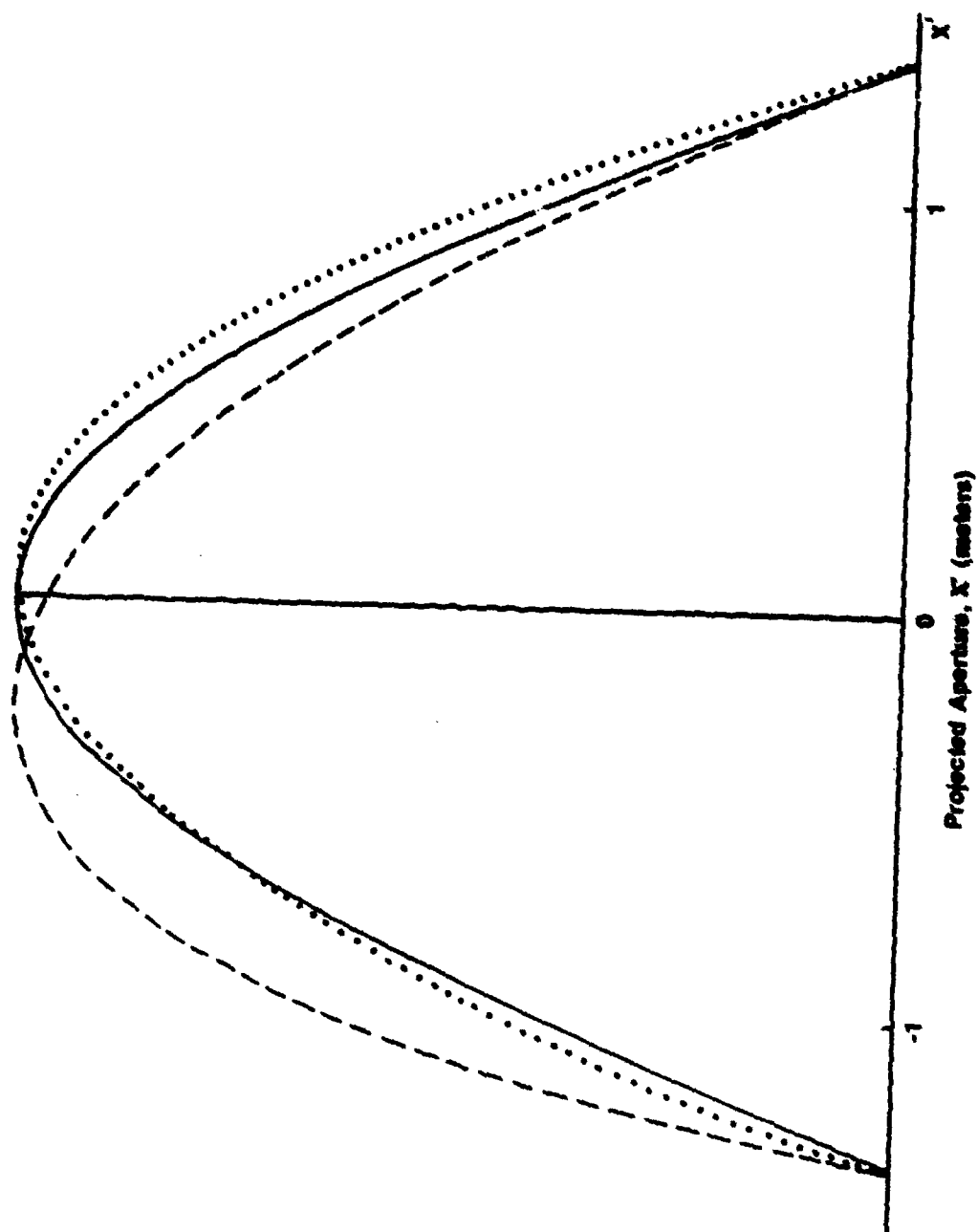Projected Aperture, X' (meters)

13

Figure 7b. Amplitude at the Aperture in the Projection Plane at Scan Angle, θ_o, and Curvature, S/R. The solid line is for the ideal cosine (planar array); the dashed line is for the distorted (curved array); and the dotted line is for the curved array with the correction. $\theta_o = 20°$, $S/R = 1.6$
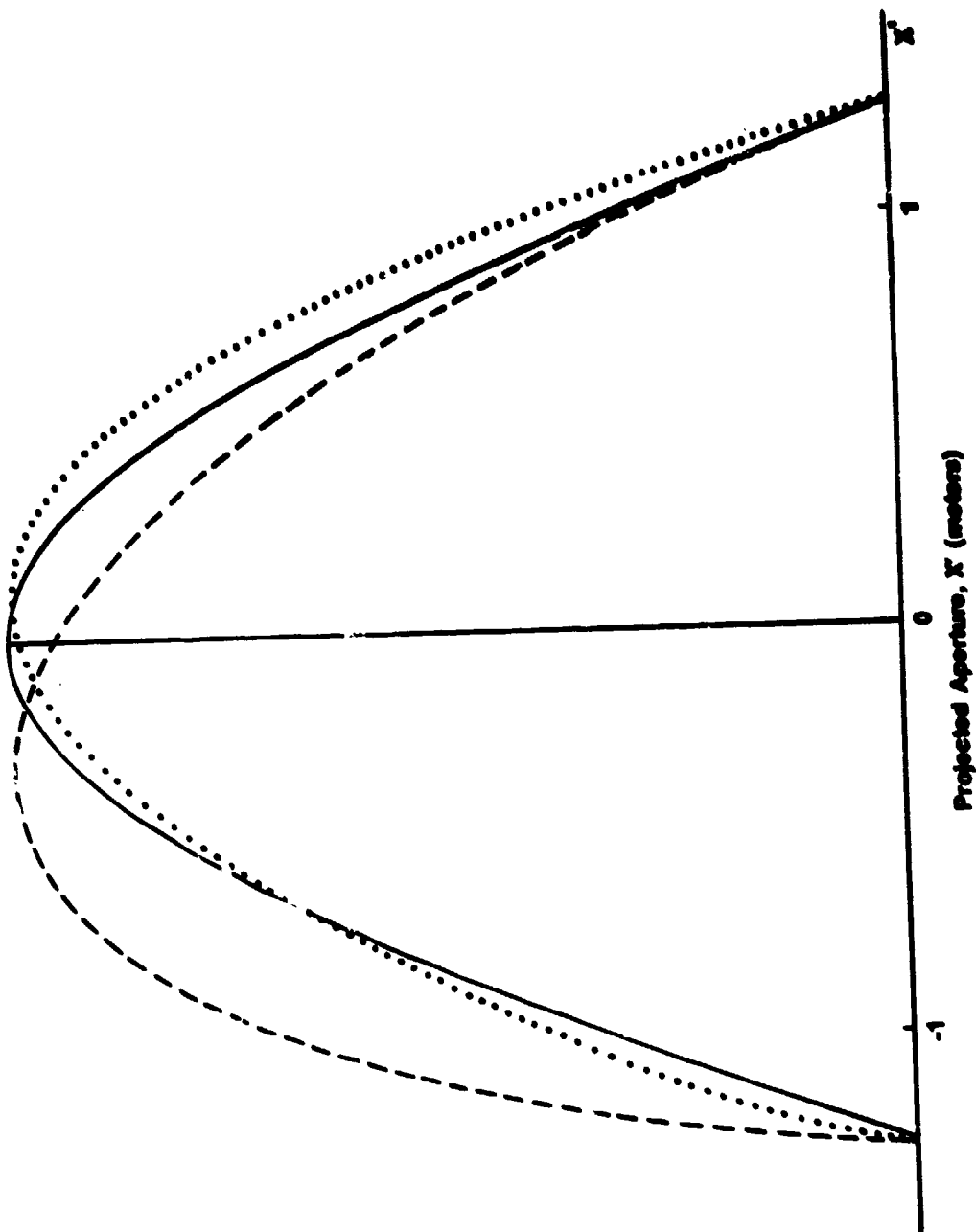
14

Figure 7c. Amplitude at the Aperture in the Projection Plane at Scan Angle, θ_0, and Curvature, S/R. The solid line is for the ideal cosine (planar array); the dashed line is for the distorted (curved array); and the dotted line is for the curved array with the correction. $\theta_0 = 20°$, S/R = 2

15

Figure 7d. Amplitude at the Aperture in the Projection Plane at Scan Angle, θ_o and Curvature, S/R. The solid line is for the ideal cosine (planar array): the dashed line is for the distorted (curved array): and the dotted line is for the curved array with the correction. $\theta_o = 30°$, $S/R = 1.07$
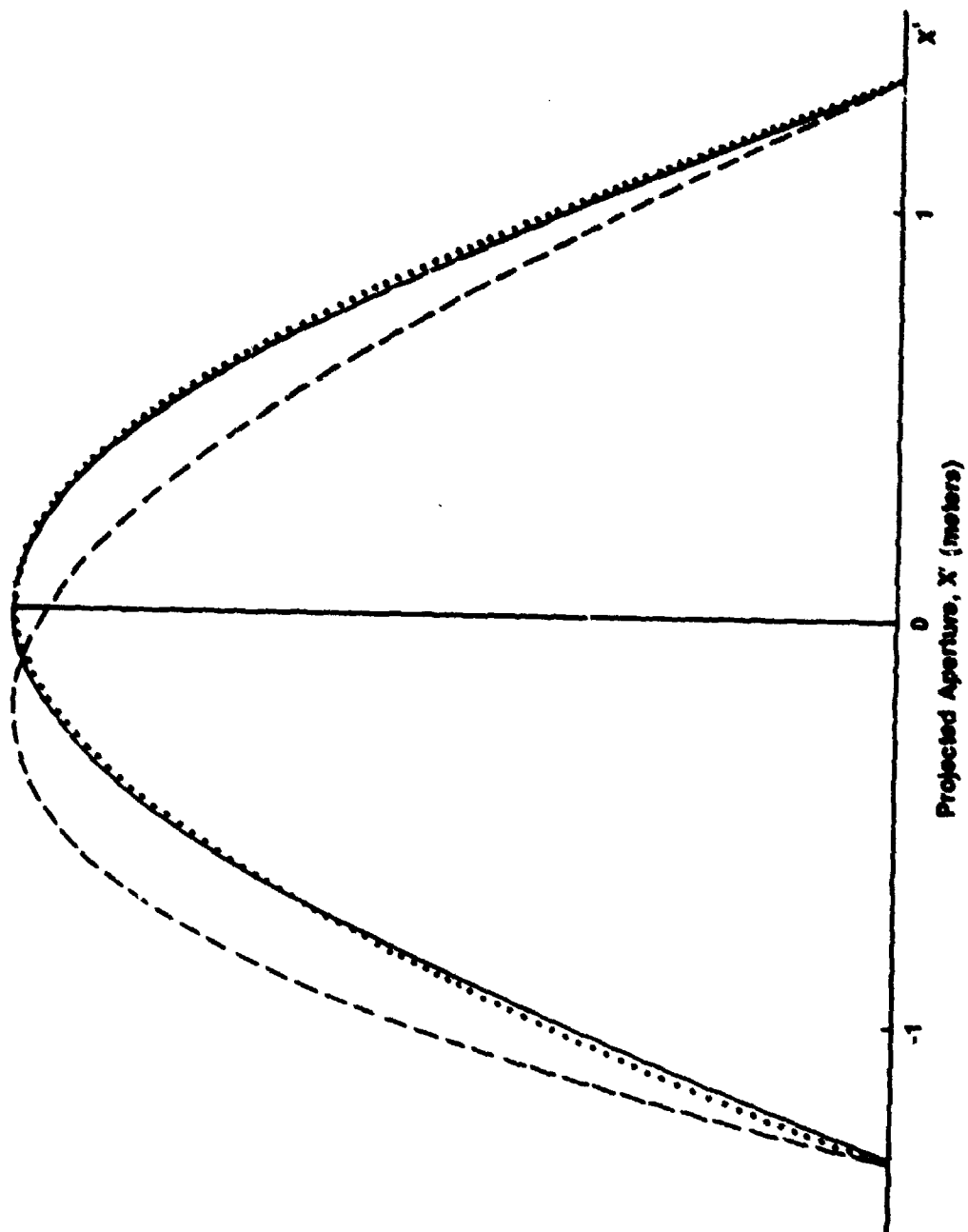
16

Figure 7e. Amplitude at the Aperture in the Projection Plane at Scan Angle, θ_0, and Curvature, S/R. The solid line is for the ideal cosine (planar array); the dashed line is for the distorted (curved array); and the dotted line is for the curved array with the correction. $\theta_0 = 30°$, $S/R = 1.6$

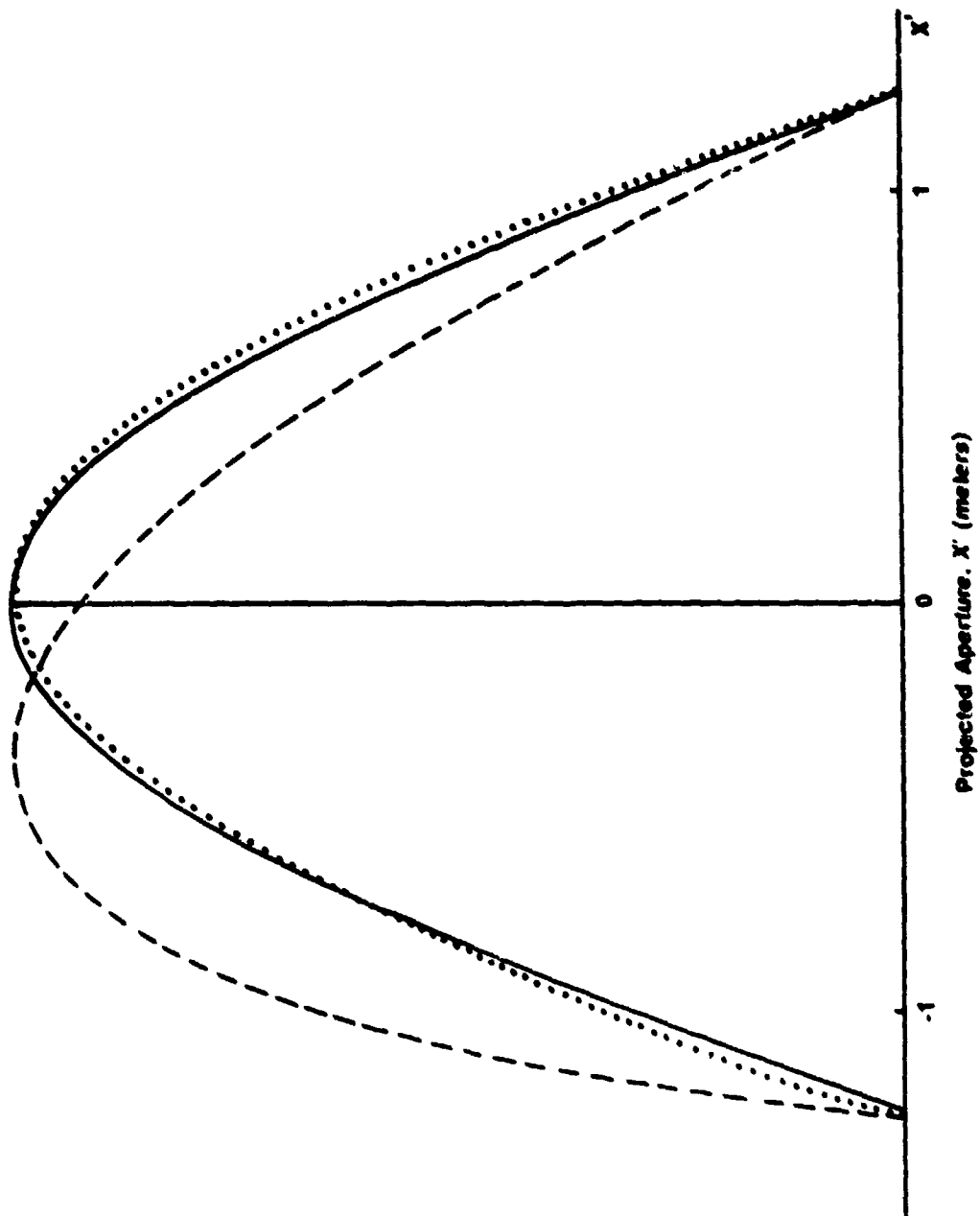Projected Aperture, X' (meters)

Figure 7f. Amplitude at the Aperture in the Projection Plane at Scan Angle, θ, and Curvature, S/R. The solid line is for the ideal cosine (planar array); the dashed line is for the distorted (curved array); and the dotted line is for the curved array with the correction. $\theta_s = 30°$, S/R = 2
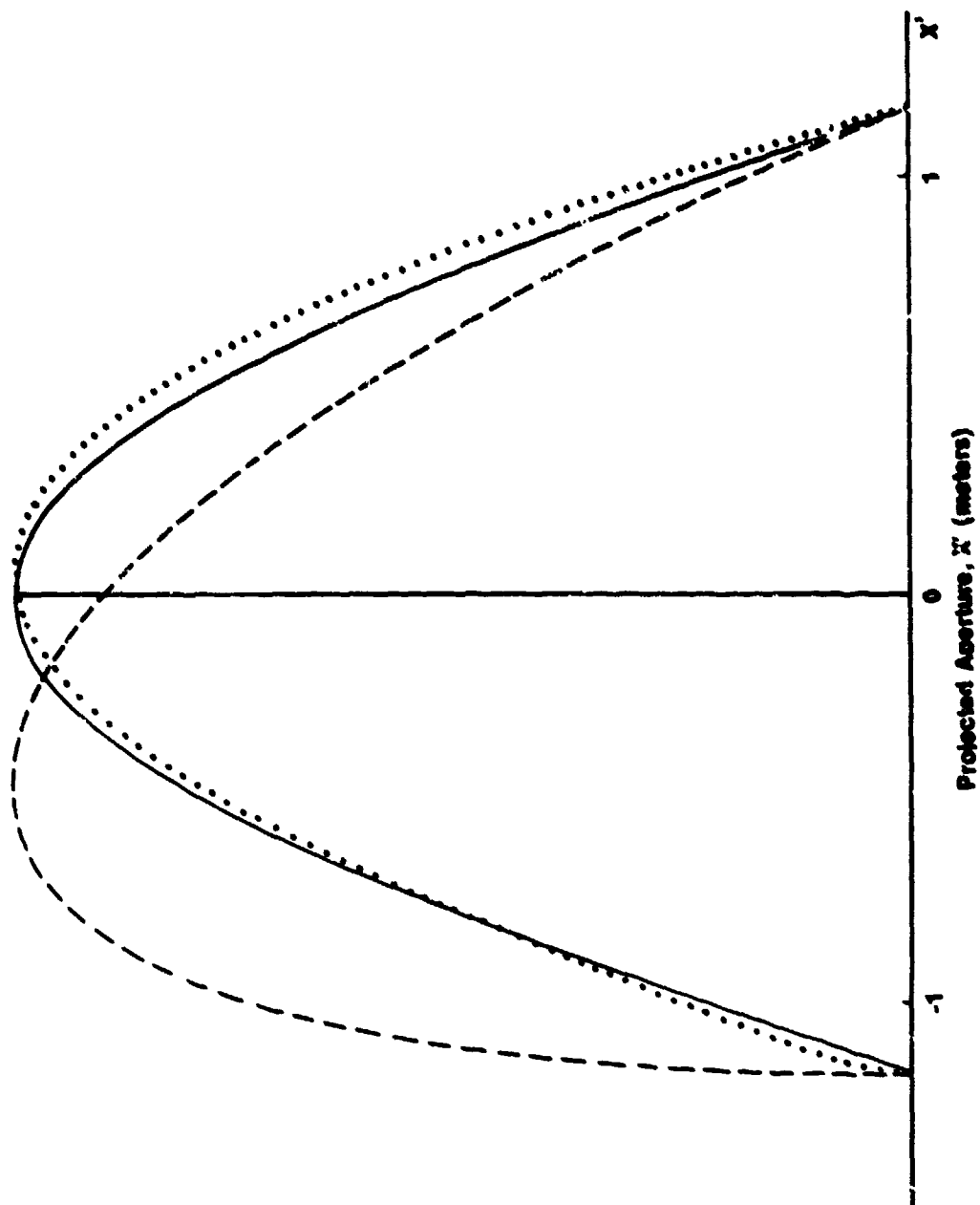
13

Figure 7g. Amplitude at the Aperture in the Projection Plane at Scan Angle, θ_0, and Curvature, S/R. The solid line is for the ideal cosine (planar array); the dashed line is for the distorted (curved array); and the dotted line is for the curved array with the correction. $\theta_0 = 40°$, S/R = 1.07
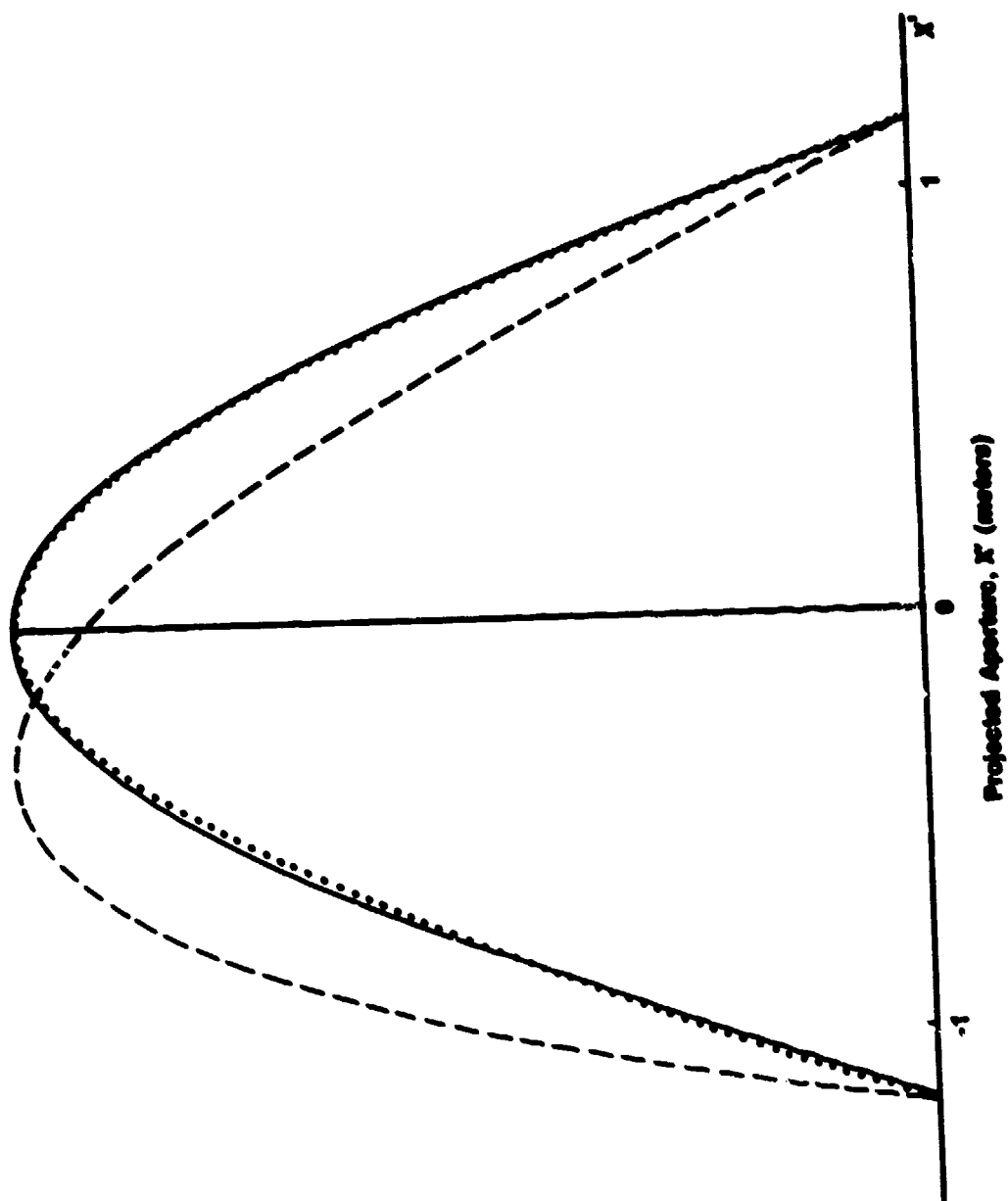
Projected Aperture, X' (meters)

Figure 7h. Amplitude at the Aperture in the Projection Plane at Scan Angle, θ_o, and Curvature, S/R. The solid line is for the ideal cosine (planar array); the dashed line is for the distorted (curved array); and the dotted line is for the curved array with the correction. $\theta_o = 40°$, S/R = 1.6

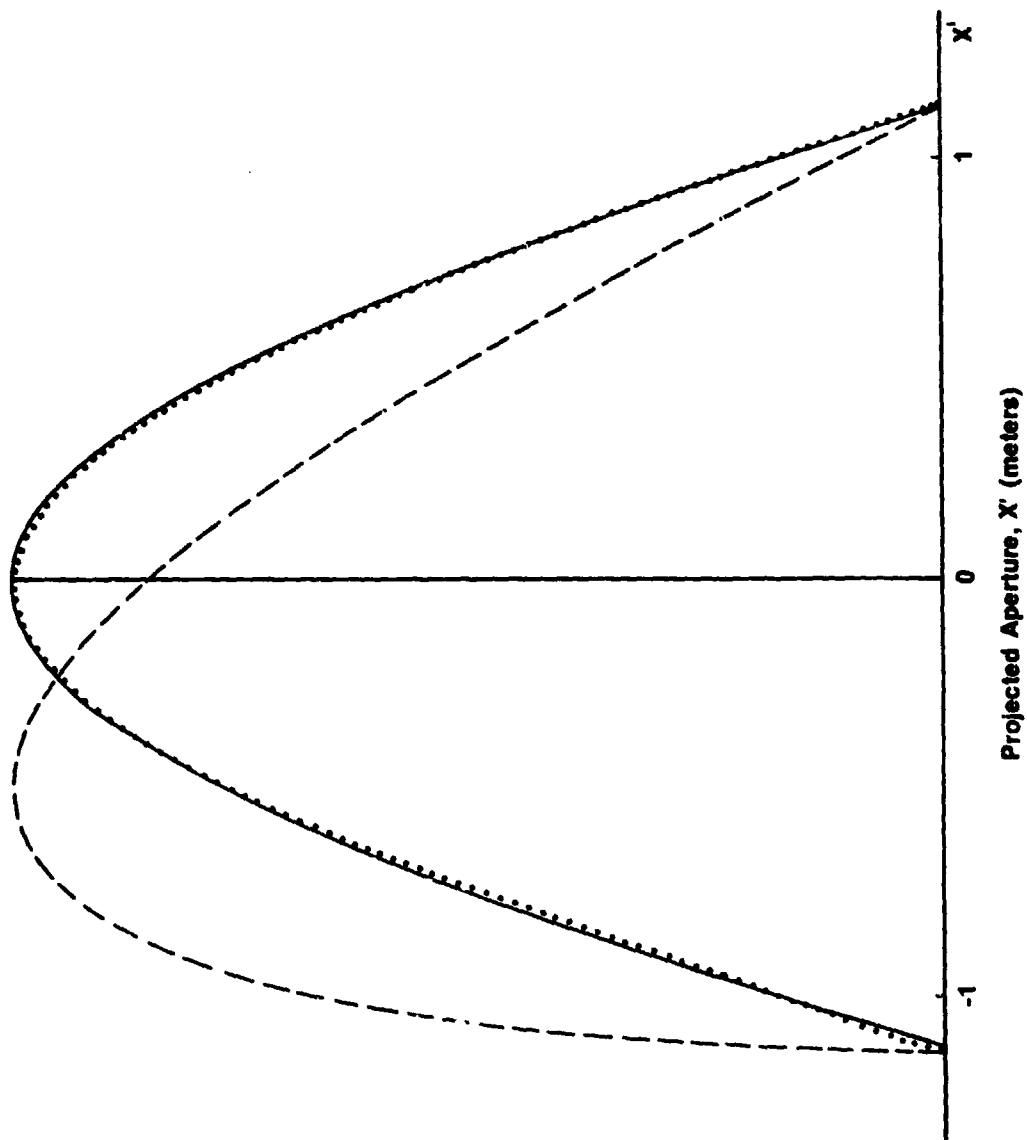# 4. CURVATURE EFFECTS ON RADIATION PATTERN

4.1 Scanning Radiation Pattern of Array on Curved Surface and Its Correction Factor

The power radiated at an arbitrary scan angle, θ_o, can be obtained by considering the scan angle direction of each element, and taking into account the path length difference of each element. The E-field in the scan angle direction, θ_o, is:

$$E(\theta_o) = \sum_{n=-K/2}^{K/2} A_e(n, \theta_o) A_n e^{j\phi_n} e^{-jkz_n(\theta_o)} \tag{19}$$

where $k = 2\pi/\lambda$, and A_n and ϕ_n are the magnitude and phase respectively of the nth element's excitation coefficient. A_n is the amplitude taper across the aperture, usually referred to as the aperture taper. $Z_n(\theta_o)$ is the nth element's path length difference from a reference element; here the reference element is the center element. $A_e(n, \theta_o)$ is the nth element's amplitude due to the element radiation pattern in the direction of θ_o.

$$A_e(n, \theta_o) = \cos^p(\theta_0 - ns/R) \tag{20}$$

p being a constant defining the element pattern. A beam is steered to the θ_o direction by having ϕ_n equal to $kZ_n(\theta_o)$. The value of $Z_n(\theta_o)$ is computed from the following derived equation:

$$Z_n(\theta_o) = 2R \sin(ns/2R) \cos(\pi/2 - \theta_o + ns/2R) . \tag{21}$$

The E-field in the θ direction, relative to a θ_o scan angle direction is:

$$E(\theta) = \sum_{n=-K/2}^{K/2} A_e(n, \theta) A_n e^{jkz_n(\theta_o)} e^{-jkz_n(\theta)} \tag{22}$$

where A_n is real and ϕ_n has been set equal to $kZ_n(\theta_o)$. $A_e(n, \theta)$ and $Z_n(\theta)$ are given by Eqs. (20) and (21) respectively, using θ in place of θ_o.

The value of the power, P, is obtained by using Eq. (22) in the following equation:

$$P = \frac{1}{2} \left| E(\theta) \right|^2 . \tag{23}$$

21

The effect of curvature on the radiation pattern is predominantly a function of θ_o, ns/r, and, consequently, Ks/R or S/R, the array's subtended angle. To demonstrate the effect of curvature, the radiation pattern, P, is obtained as a function of S/R (with θ_o constant), and as a function of θ_o (with S/R constant). Both the number of elements, K + 1, and the element spacing, s, are held constant. The effect of curvature is diminished by adjusting the aperture taper, A_n. For the case of a cosine aperture taper,

$$A_n = \cos(\pi n/K) . \tag{24}$$

In Section 2.3 it was found that the cosine taper distortion was measured according to Eq. (11). The distortion was corrected by using A'_n in place of A_n, such that

$$A_n = \sqrt{1 - B^2} \; \cos\left(\frac{\pi n}{K}\right) + B \sin\left(\frac{2\pi n}{K}\right) \tag{25}$$

using A_n in place of A_n in Eq. (22), the corrected power pattern is obtained.

4.2 Radiation Pattern Using a $\cos^{1.5}(\theta)$ Element Pattern

The $\cos^{1.5}(\theta)$ element pattern is a practical case since a patch radiator, a slot, or a dipole in an array exhibits very nearly this dependency. Figures 8a through 8h show the radiation plots using $\cos^{1.5}(\theta)$ element pattern and cosine aperture taper for various values of scan angle, θ_o, and subtended angle, S/R. The number of elements used is 65, the element spacing is $\lambda/2$ and λ is 0.1 meters. The correction is most pronounced as the scan angle is increased and/or the subtended angle is increased. The figures show the increase of the near-in sidelobe levels as a function of scan angle, and subtended angle; the uncorrected and corrected patterns are shown. The improvement of the distorted pattern is substantial, showing the correction works well. The pattern is very much restored in the near-in sidelobes. Moreover, there is no detriment in the corrected pattern in the rest of the 360° coverage. There is a greater improvement in the larger scan angles, as was predicted from the discussion on errors.
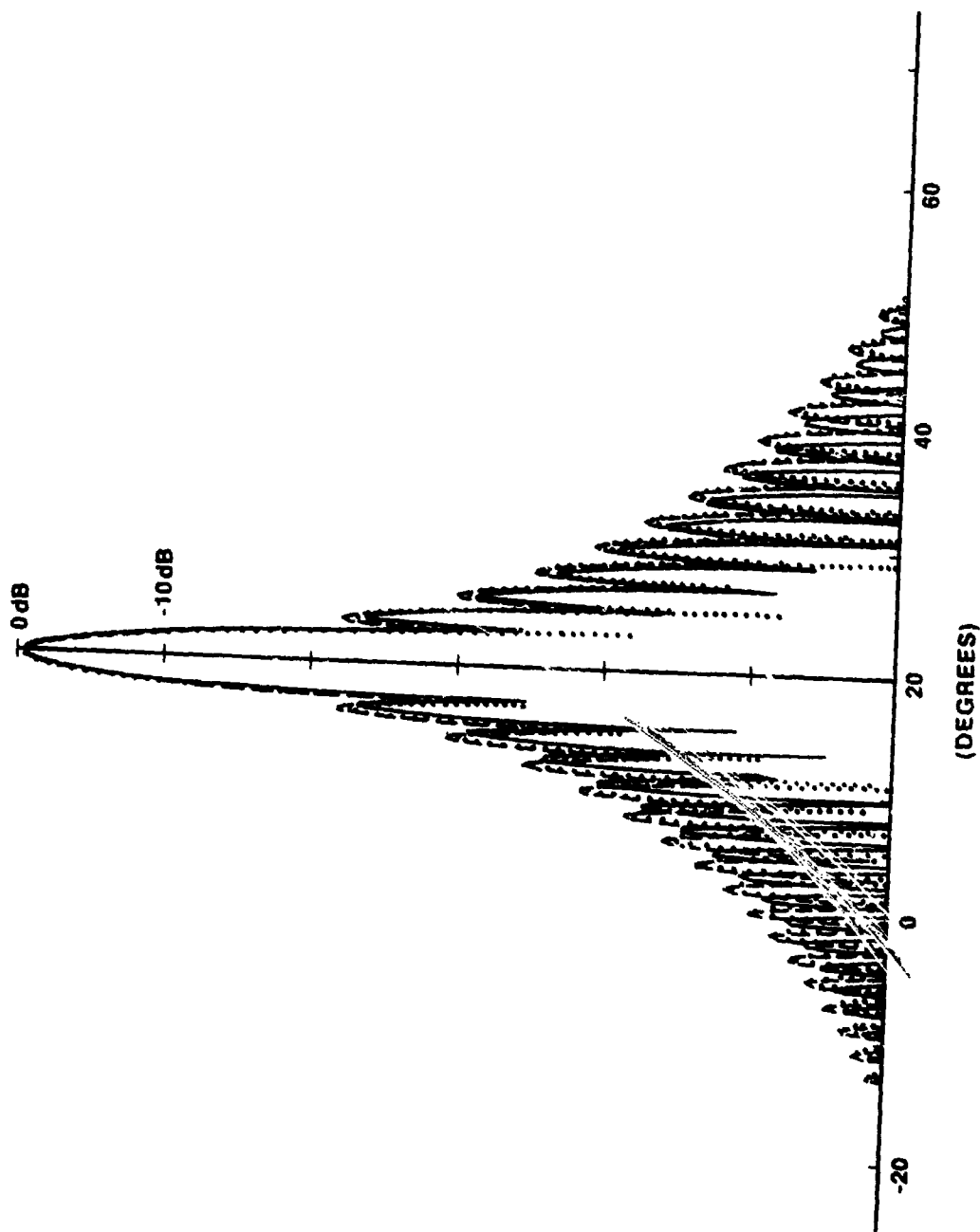
Figure 8a. Radiation Pattern Showing $\pm 45°$ Off of the Scan Angle, θ_O. A $\cos^{1.5}(\theta)$ element pattern and a cosine illumination are used. The solid line is for the planar array; the dashed line is for the curved array; and the dotted line is for the curved array with the correction. $\theta_O = 20°$, $S/R = 1.07$
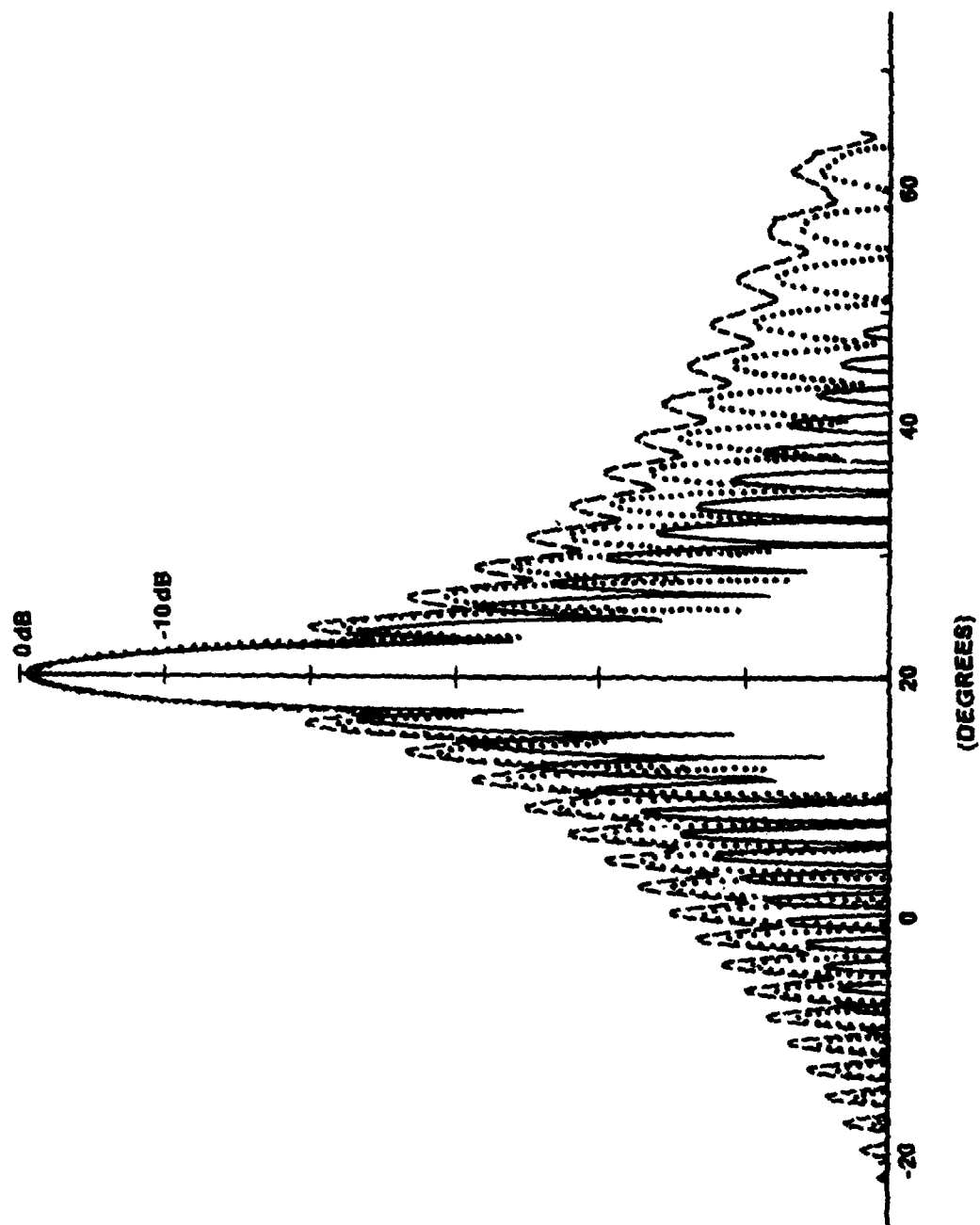
Figure 8b. Radiation Pattern Showing ±45° Off of the Scan Angle, θ_o. A $\cos^{1.5}(\theta)$ element pattern and a cosine illumination are used. The solid line is for the planar array; the dashed line is for the curved array; and the dotted line is for the curved array with the correction. $\theta_o = 20°$, $S/R = 1.6$
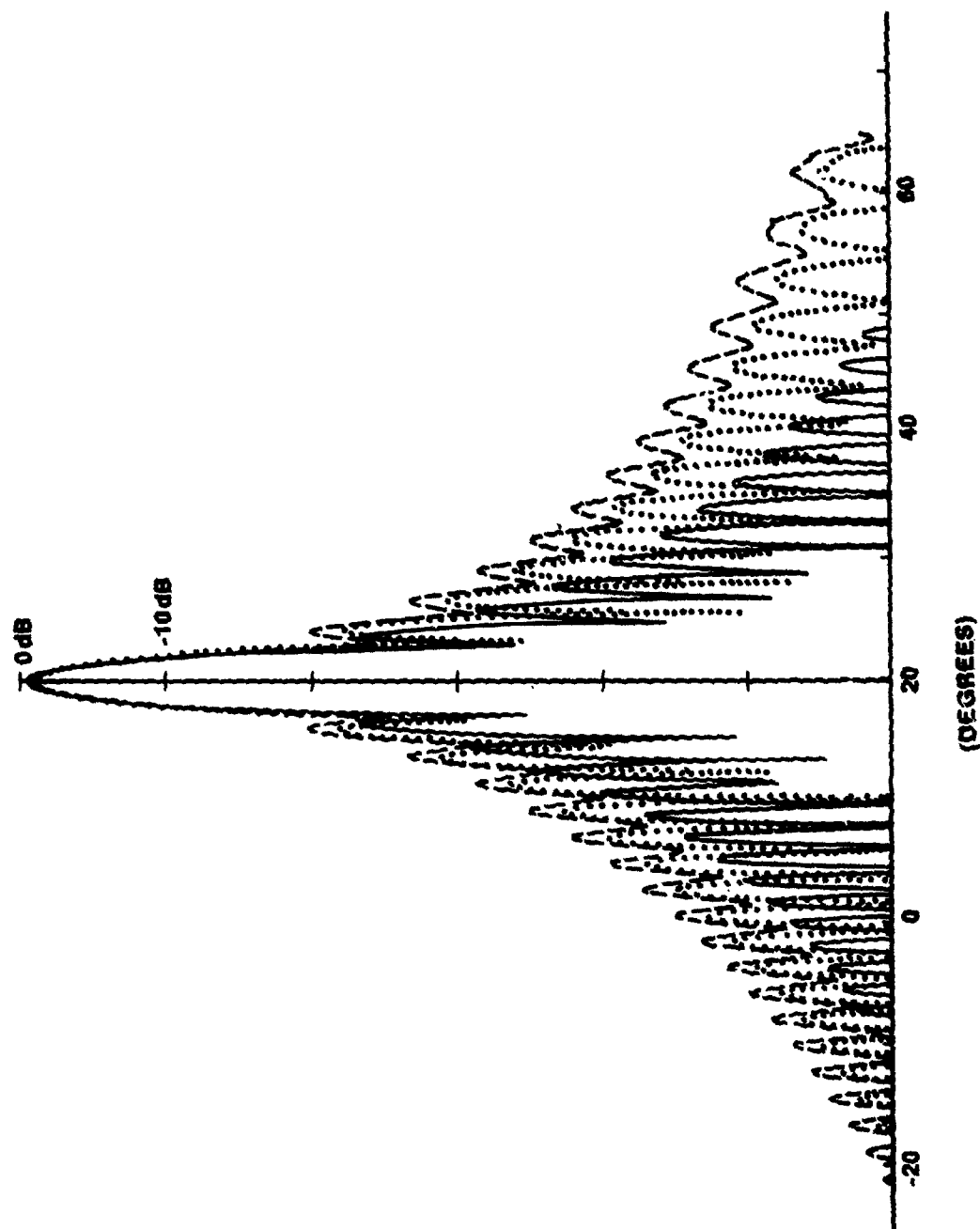
24

Figure 8c. Radiation Pattern Showing ±45° Off of the Scan Angle, θ_o. A $\cos^{1.5}(\theta)$ element pattern and a cosine illumination are used. The solid line is for the planar array; the dashed line is for the curved array; and the dotted line is for the curved array with the correction. $\theta_o = 20°$, $S/R = 2$
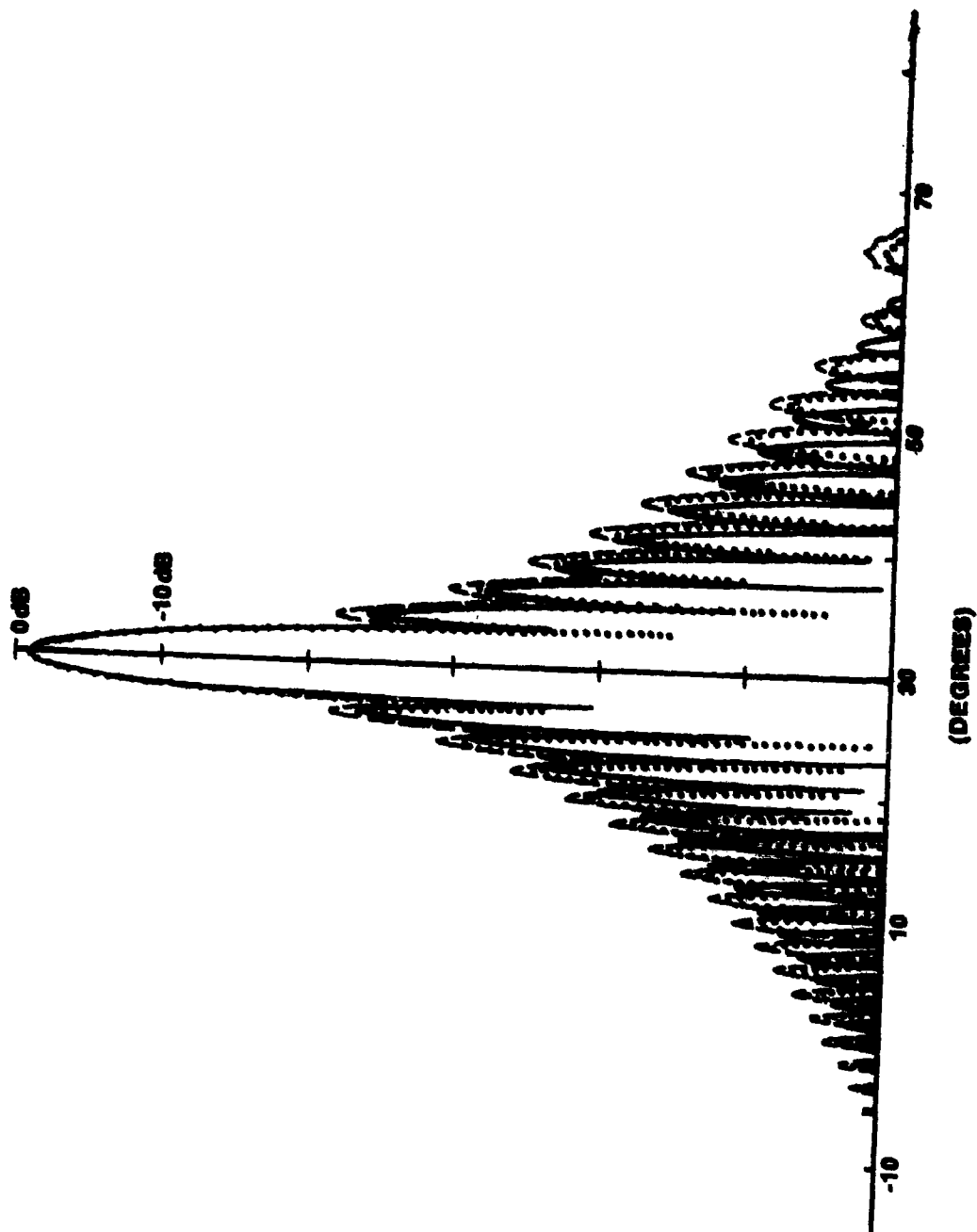
Figure 8d. Radiation Pattern Showing ±45° Off of the Scan Angle, θ_o. A $\cos^{1.5}(\theta)$ element pattern and a cosine illumination are used. The solid line is for the planar array; the dashed line is for the curved array; and the dotted line is for the curved array with the correction. $\theta_o = 30°$, $S/R = 1.07$

Figure 8e. Radiation Pattern Showing ±45° Off of the Scan Angle, θ_o. A $\cos^{1.5}(\theta)$ element pattern and a cosine illumination are used. The solid line is for the planar array; the dashed line is for the curved array; and the dotted line is for the curved array with the correction. $\theta_o = 30°$, $S/R = 1.6$
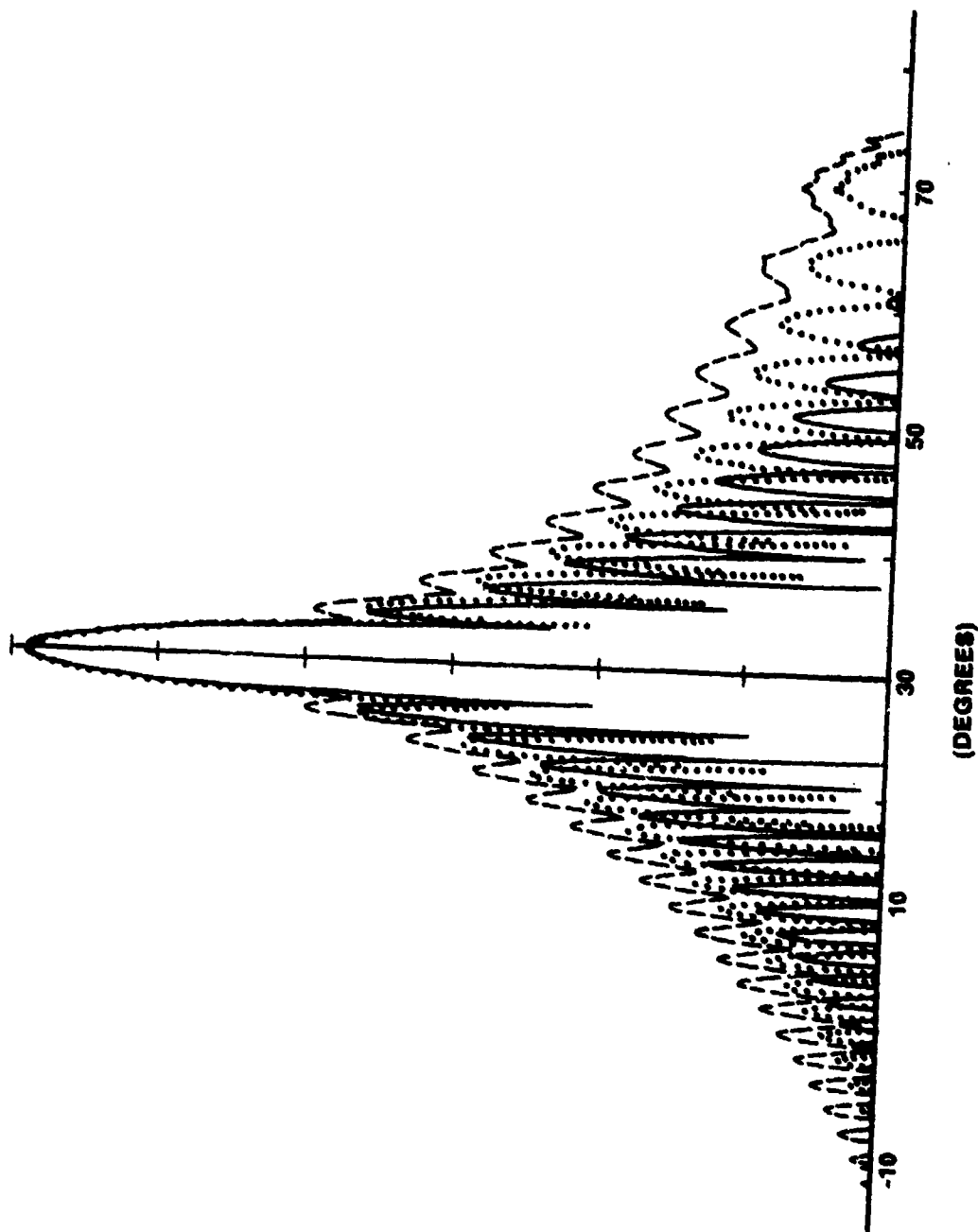
(DEGREES)

27

Figure 8f. Radiation Pattern Showing ±45° Off of the Scan Angle, θ_0. A $\cos^{1.5}(\theta)$ element pattern and a cosine illumination are used. The solid line is for the planar array; the dashed line is for the curved array; and the dotted line is for the curved array with the correction. $\theta_0 = 30°$, $S/R = 2$
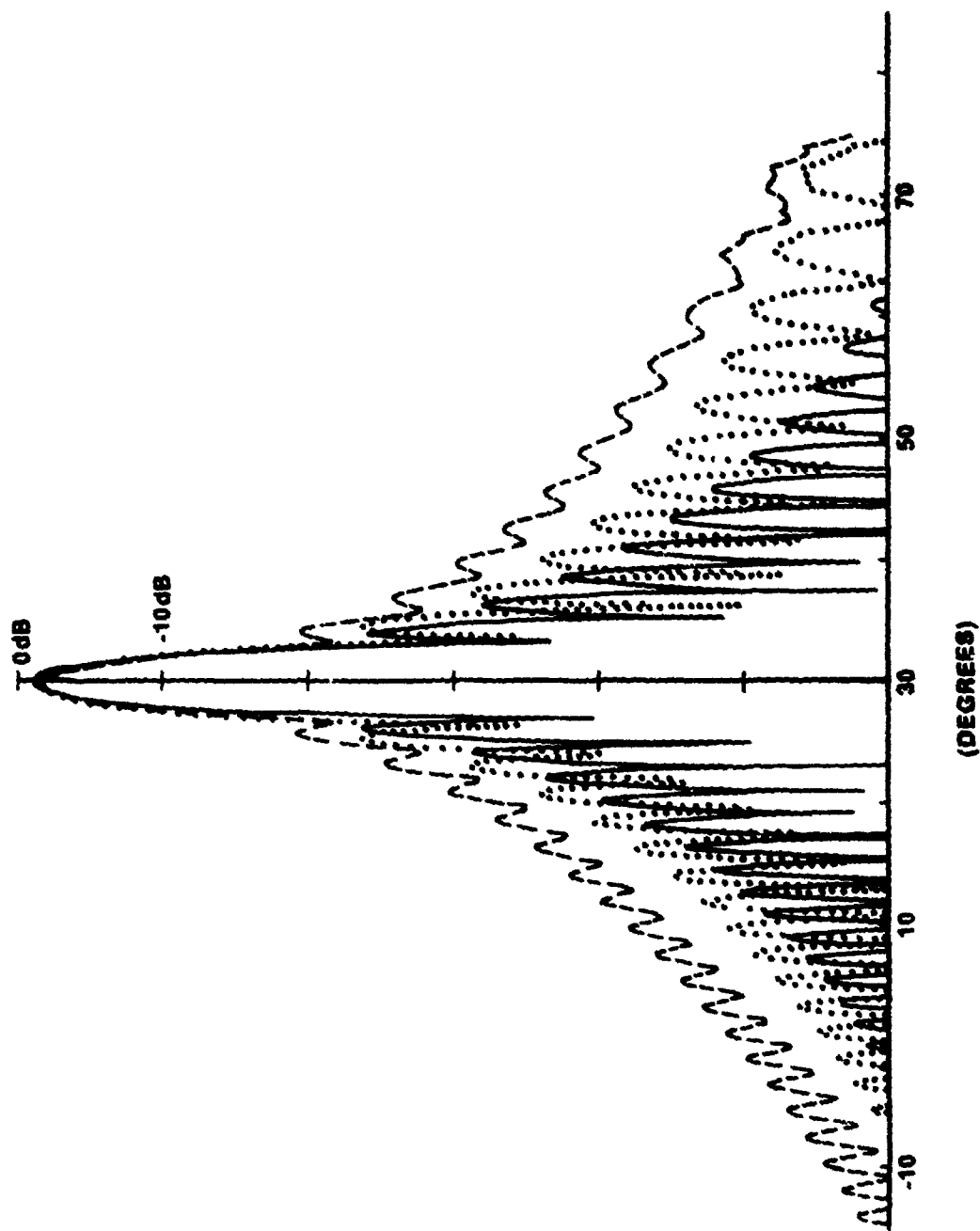
Figure 8g. Radiation Pattern Showing ±45° Off of the Scan Angle, θ_o. A $\cos^{1.5}(\theta)$ element pattern and a cosine illumination are used. The solid line is for the planar array; the dashed line is for the curved array; and the dotted line is for the curved array with the correction. $\theta_o = 40°$, S/R = 1.07
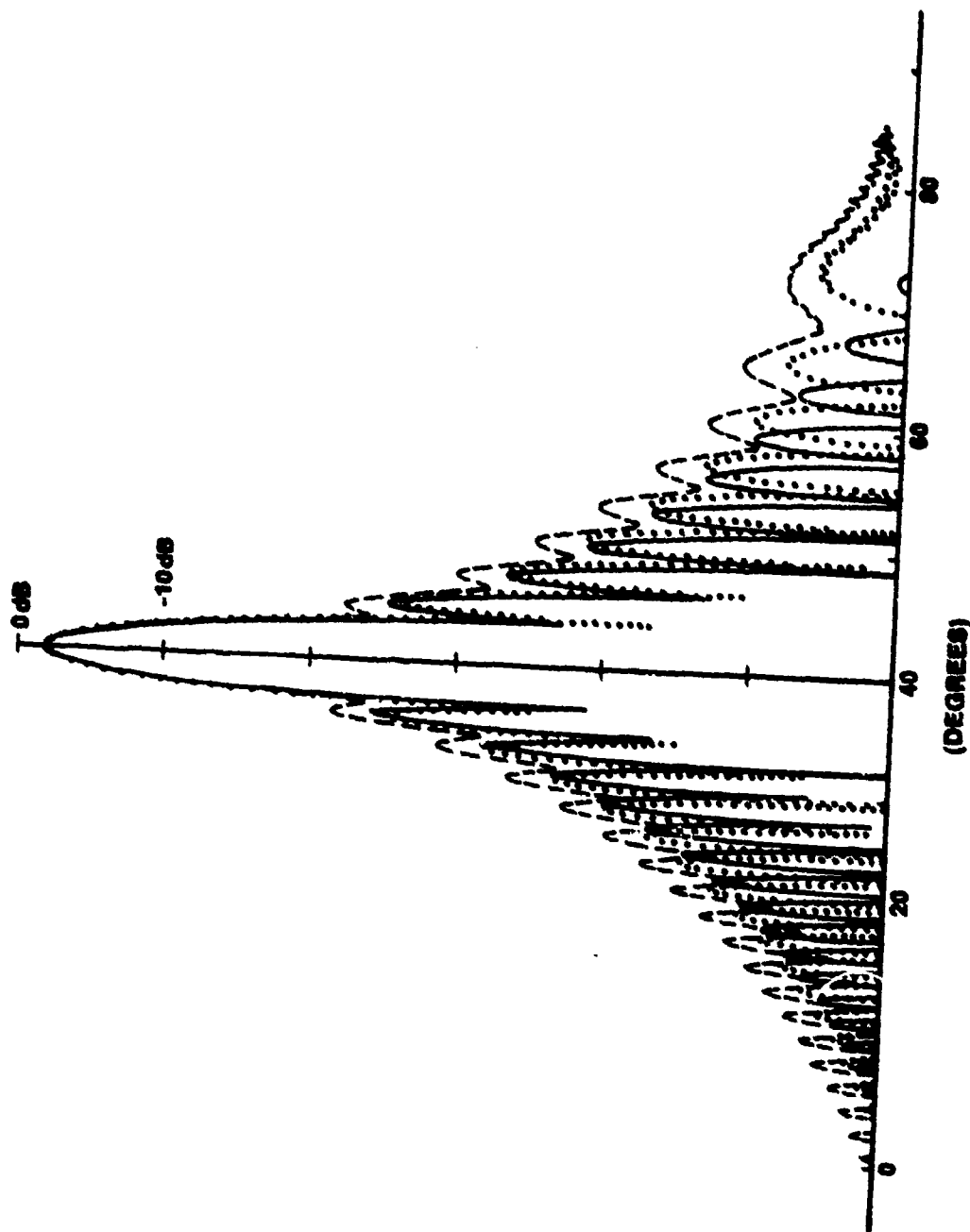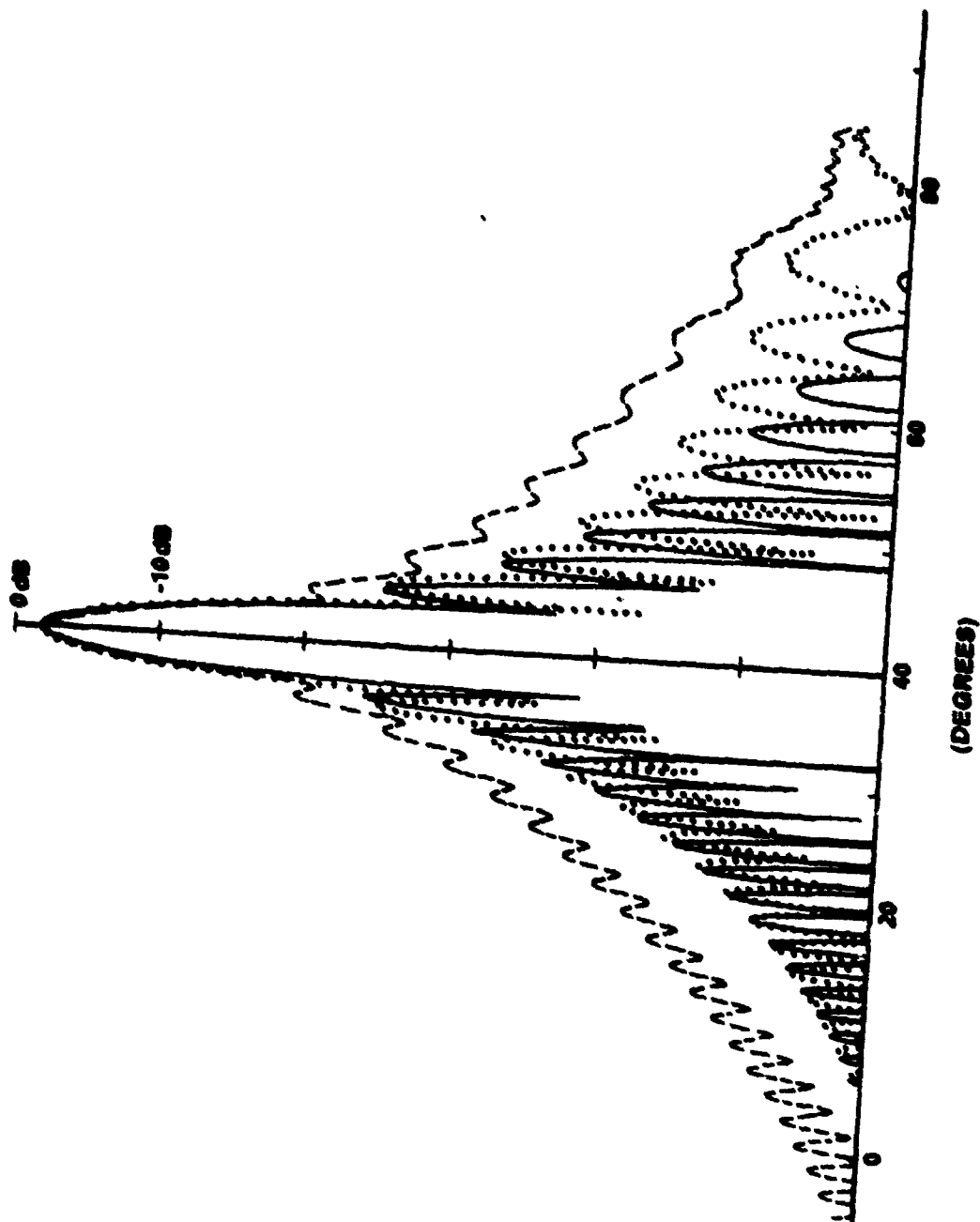
Figure 8h. Radiation Pattern Showing ±45° Off of the Scan Angle, θ_o. A $\cos^{1.5}(\theta)$ element pattern and a cosine illumination are used. The solid line is for the planar array, the dashed line is for the curved array; and the dotted line is for the curved array with the correction. $\theta_o = 40°$, $S/R = 1.6$

4.3 The Difference Pattern

The difference pattern was not discussed earlier because it is not the primary subject of the investigation. The difference pattern is obtained from the other port, which is part of the difference channel between the receiver and the variable power divider. If the transmitted signal amplitude at the sum and difference output ports, after the power divider, are A and B respectively, then a received signal at the difference channel, will be the addition of the amplitude B, now from the sum network, and minus A from the difference network. When the correction, B_0, is employed, the amplitude used for the calculation of the difference pattern is:

$$A_n = B_0 \cos\left(\frac{\pi n}{K}\right) - \sqrt{1 - B_0^2} \; \sin\left(\frac{2\pi n}{K}\right). \qquad (26)$$

The application of the correction for the optimum sum pattern results in an improvement of the difference pattern. The crucial criterion of a difference pattern is the mainbeam null depth; the deeper the mainbeam null, the better the pattern. One example of the improvement of the difference pattern is shown in Figure 9.

Table 2 depicts the improvement of the mainbeam null depth that can be seen to be significant. The improvement decreases slowly as the curvature increases. There is not a significant variation with a change of the scan angle. A better difference pattern can be obtained by sacrificing some of the correction of the sum pattern.

Table 2. Values of Mainbeam Null of Uncorrected and Corrected Difference Patterns as a Function of Scan Angle and Subtended Angle. A $\cos^{1.5}(\theta)$ element pattern was used

θ_o	$\frac{S}{R}$	MAINBEAM NULL (-dB)		IMPROVEMENT IN dB
		UNCORRECTED PATTERN	CORRECTED PATTERN	
20°	1.07	23.20	30.66	7.46
	1.6	19.70	25.72	6.02
	2	17.78	22.50	4.72
30°	1.07	19.71	27.35	7.64
	1.6	16.20	22.40	6.20
	2	14.24	19.27	5.03
40°	1.07	17.24	24.92	7.68
	1.06	13.68	20.06	6.38

Figure 9a. The Difference Pattern for a Scan Angle of 40°.
The Planar Array
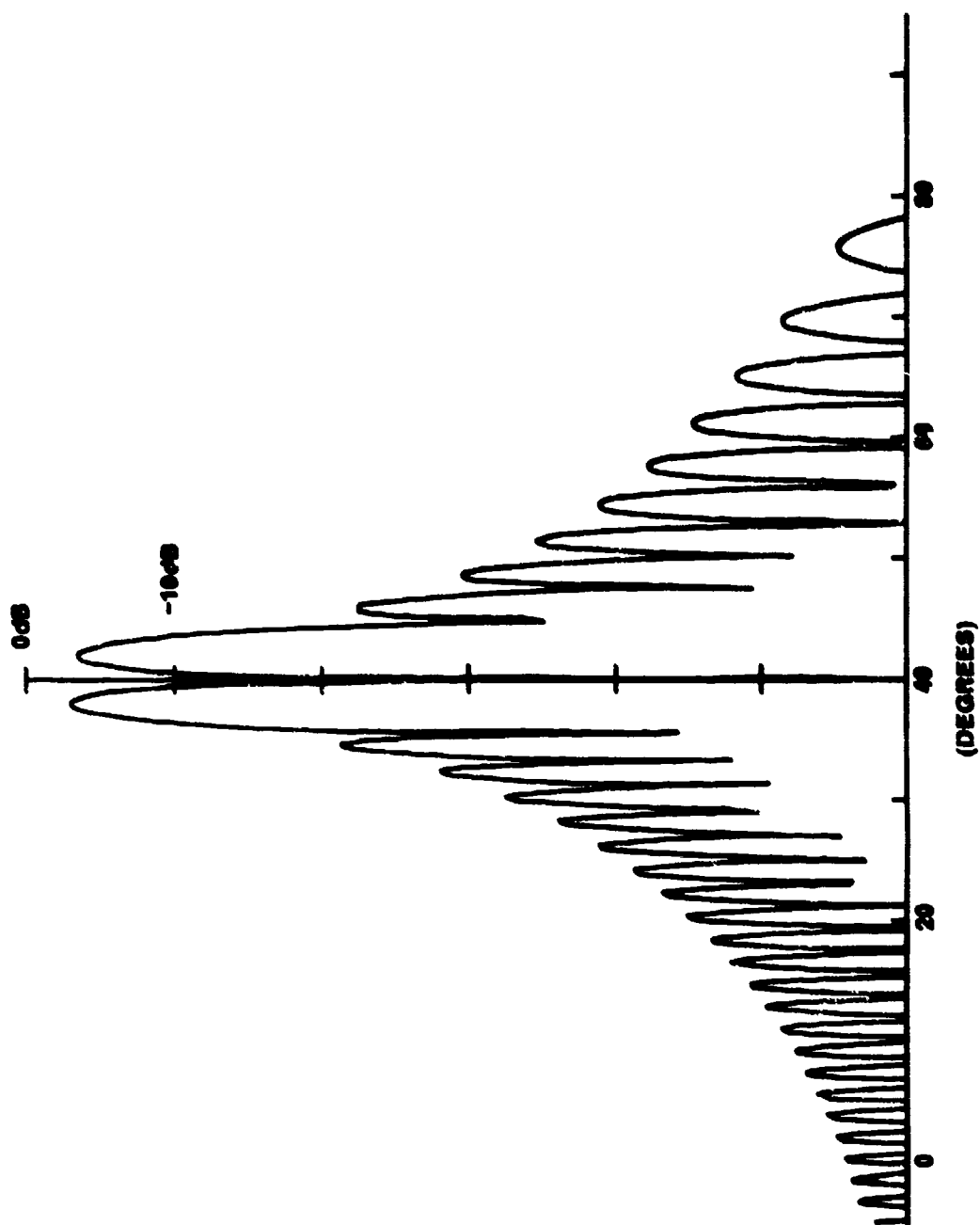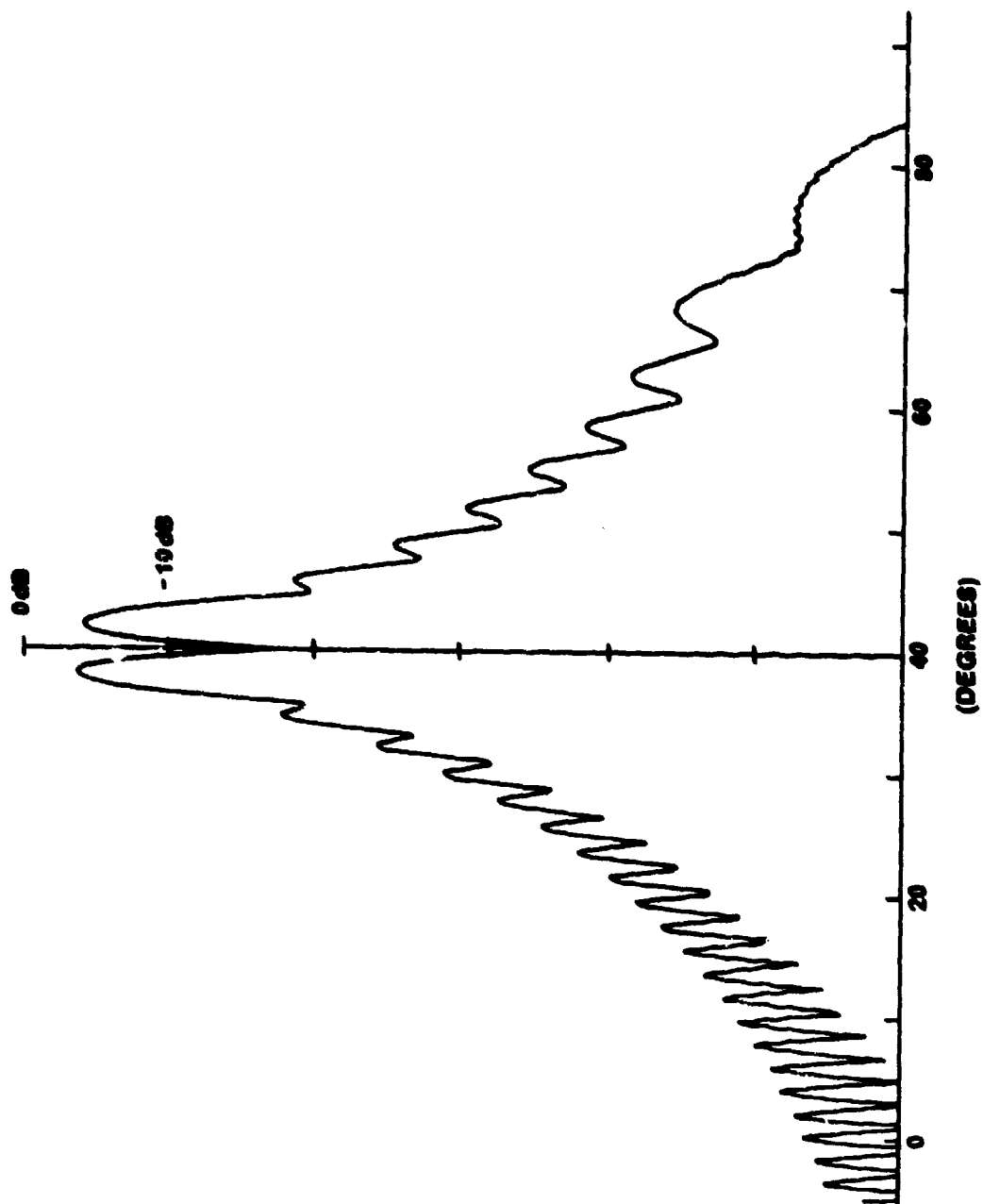
Figure 9b. The Difference Pattern for a Scan Angle of 40°.
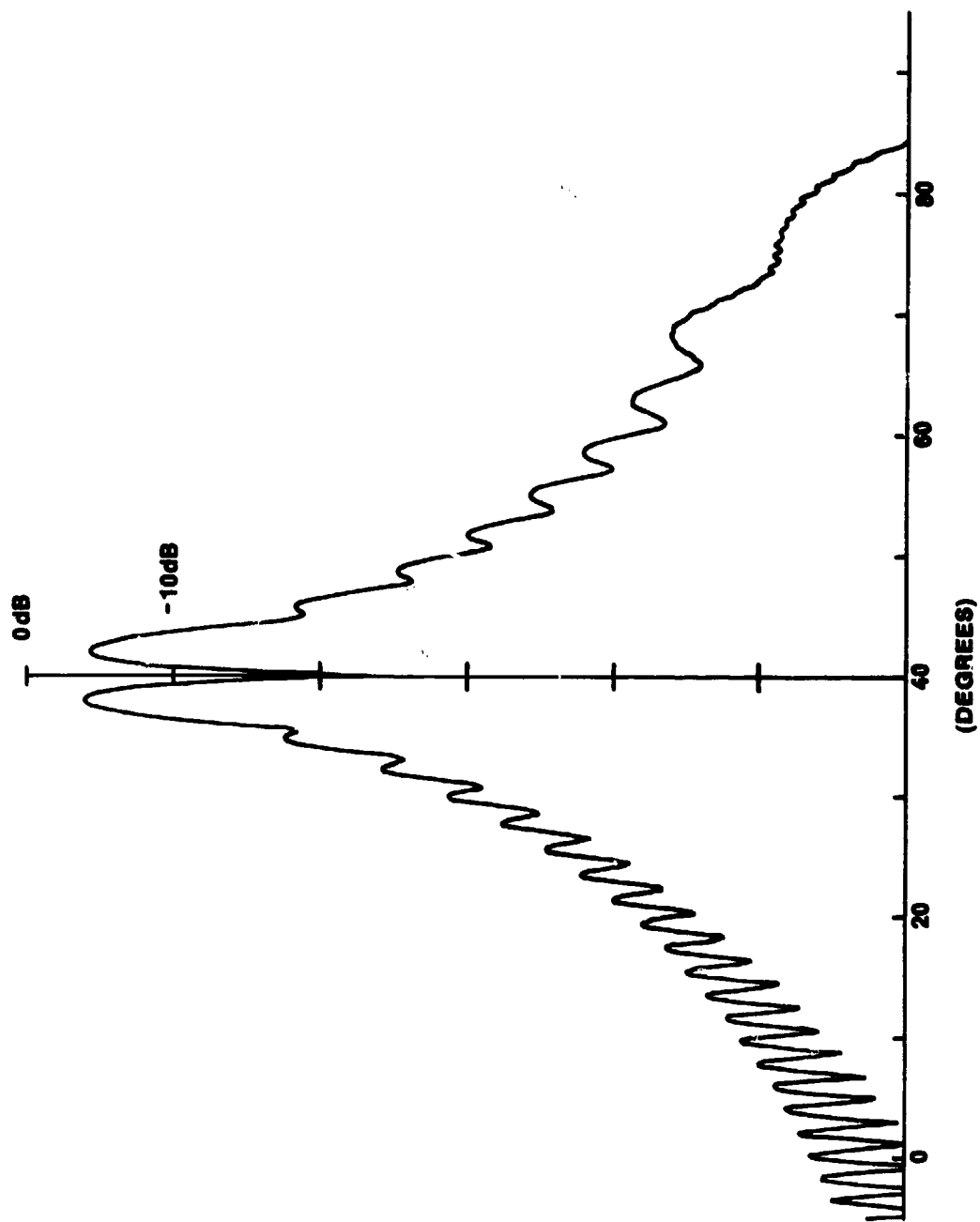A Curved Array With S/R = 1.07

33

Figure 9c. The Difference Pattern for a Scan Angle of 40°, A Curved Array With S/R = 1.07 and Using the Corrected Aperture Illumination

5. CONCLUSION

The results demonstrate the value of the correction technique. It is a simple, practical technique expending no additional power and yet offers quite a high level of improvement. It is worthwhile to compare an amplitude correction curve with a result obtained by Ludwig.[3] Ludwig used an iterative algorithm in which the complex weights of each element was adjusted in order to synthesize an ideal pattern. Although he used a Taylor aperture illumination, the two results are, to some extent, comparable. For his case, using a 40° scan angle and $S/R = 0.8$, the peak of the corrected amplitude taper shifts, in terms of his array, by about three and one-half elements. Using our technique, for $\theta_o = 40°$ and $S/R = 1.07$, there is roughly the same shift. The iterative algorithm is a synthesis technique producing an ideal set of complex weights. Our corrector approximates the comparable ideal, and, at the same time is practical and can be easily implemented in an actual system.

We demonstrated our technique using a cosine aperture taper. If a Taylor illumination was employed, we would use a Taylor, Bayliss addition. Generally, any symmetric and anti-symmetric functions are to be combined. It would be worthwhile to investigate a Taylor aperture distribution since it is a very practical case. Another study may be to use the technique in order to increase the power in the mainbeam for large scan angles. In that way, the extent of large angle scanning can be augmented and made possible by the existence of curvature. Another further study may be to investigate the possibility of using this method in order to correct for the effect of physical obstructions located within portions of the antenna's radiation field.

References

1. Wojtowicz, J., Ramsey, K.G., and Fontana, T. (1963) Conformal array analysis, Proceedings of the 1983 Antenna Applications Symposium, RADC-TR-84-52, AD A142754, Vol. 2.

2. Herper, J.C., Hessel, A., and Tomasic, B. (1985) Element pattern of an axial dipole in a cylindrical phased array, Part 1: Theory, IEEE Trans., AP-33(No. 3).

3. Ludwig, A.C. (1985) Antenna Curvature Analysis, RADC-TR-85-131, AD B097555L.

4. Rudge, A.W., Milne, K., Olver, A.D., and Knight, P. (1982) The Handbook of Antenna Design, Vol. 1, p. 490, Peter Peregrinus Ltd., London, U.K.

Appendix A

Effect of Using an Isotropic Element Pattern

The isotropic element pattern does not approximate the pattern of a known radiator in an array; however, it represents a limiting case and demonstrates when compared to the results of using other element patterns, the influence of an element pattern on curvature effects. The application of an isotropic (non varying) element pattern is now briefly examined. The subsequent calculations follow that of the $\cos^{1.5}(\theta)$ element pattern, except that the value one is used for A_e. Figure A1 shows how the error, ϵ, varies with scan angle for different values of S/R. The graphs have the same shape as Figure 6 except that the error is greater. This shows that the element pattern can be used to reduce the error. In this case, the $\cos^{1.5}(\theta)$ element pattern reduces the error, ϵ, associated with the isotropic element pattern by a factor of about 0.4. Figure A2 shows a plot of the E-field at the aperture using the isotropic element pattern. The distortion of the amplitude taper is observed to be worse than the equivalent plot using the $\cos^{1.5}(\theta)$ element pattern.
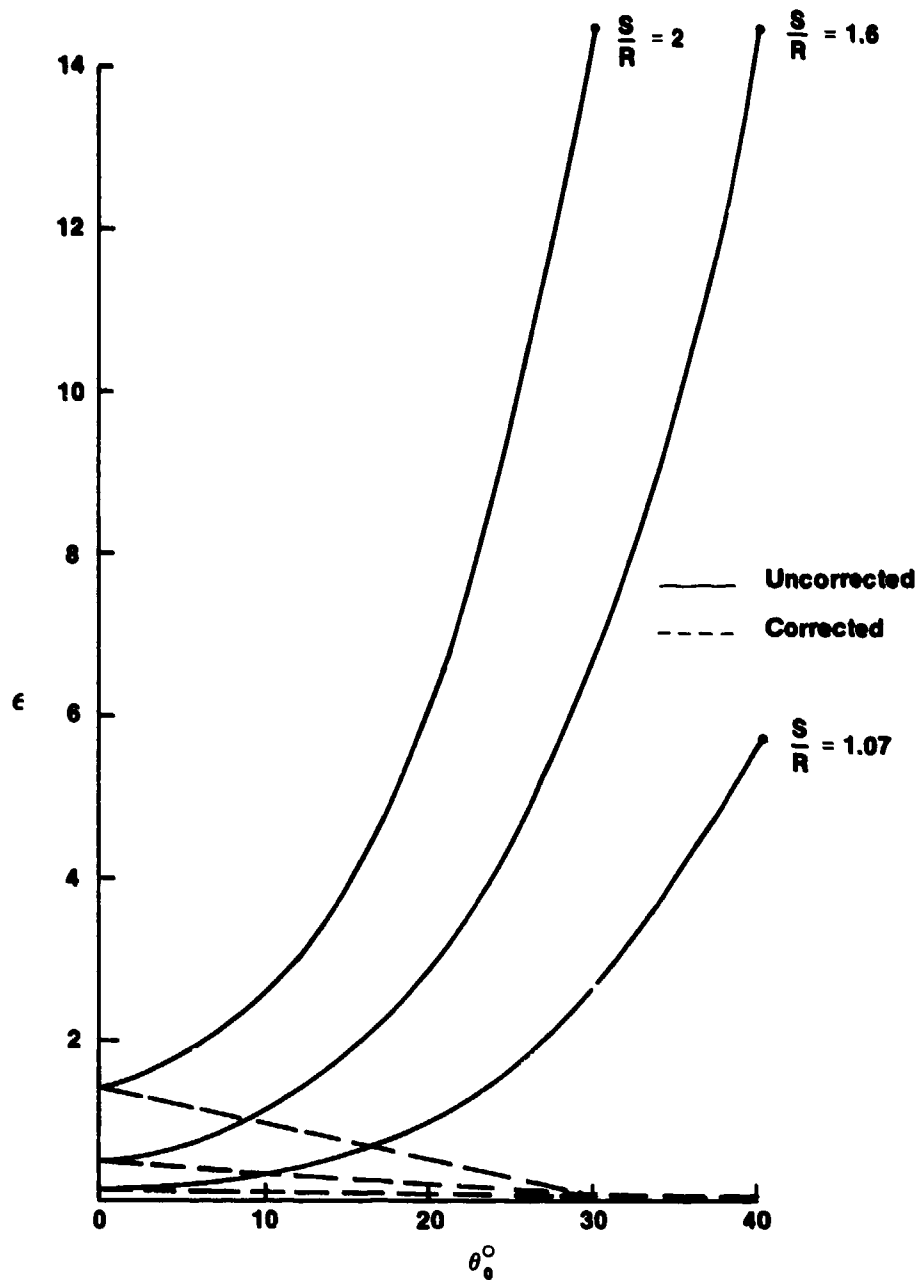
Figure A1. Error, ϵ, the Measure of the Difference Between the Distorted Curve and the Cosine Curve is Plotted as a Function of Scan Angle, θ_0, With Curvature, S/R (the subtended angle), as a Parameter. An isotropic element pattern is used
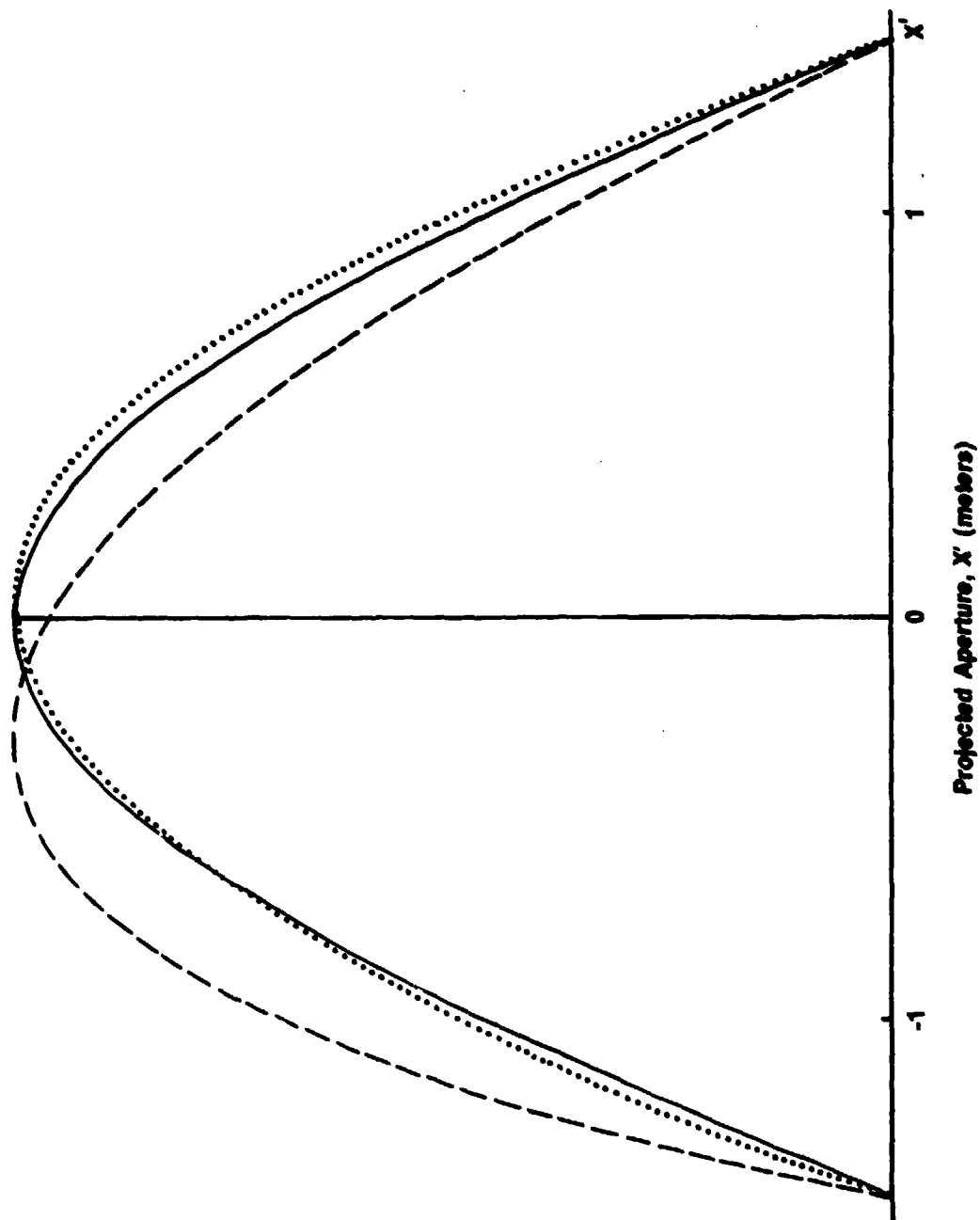
Figure A2a. Amplitude at the Aperture in the Projection Plane at Scan Angle, θ_c, and Curvature, S/R. An isotropic element pattern is used. The solid line is the ideal cosine curve; the dashed line the distorted curve; the dotted line is corrected curve. $\theta_o = 20°$, $S/R = 1.07$
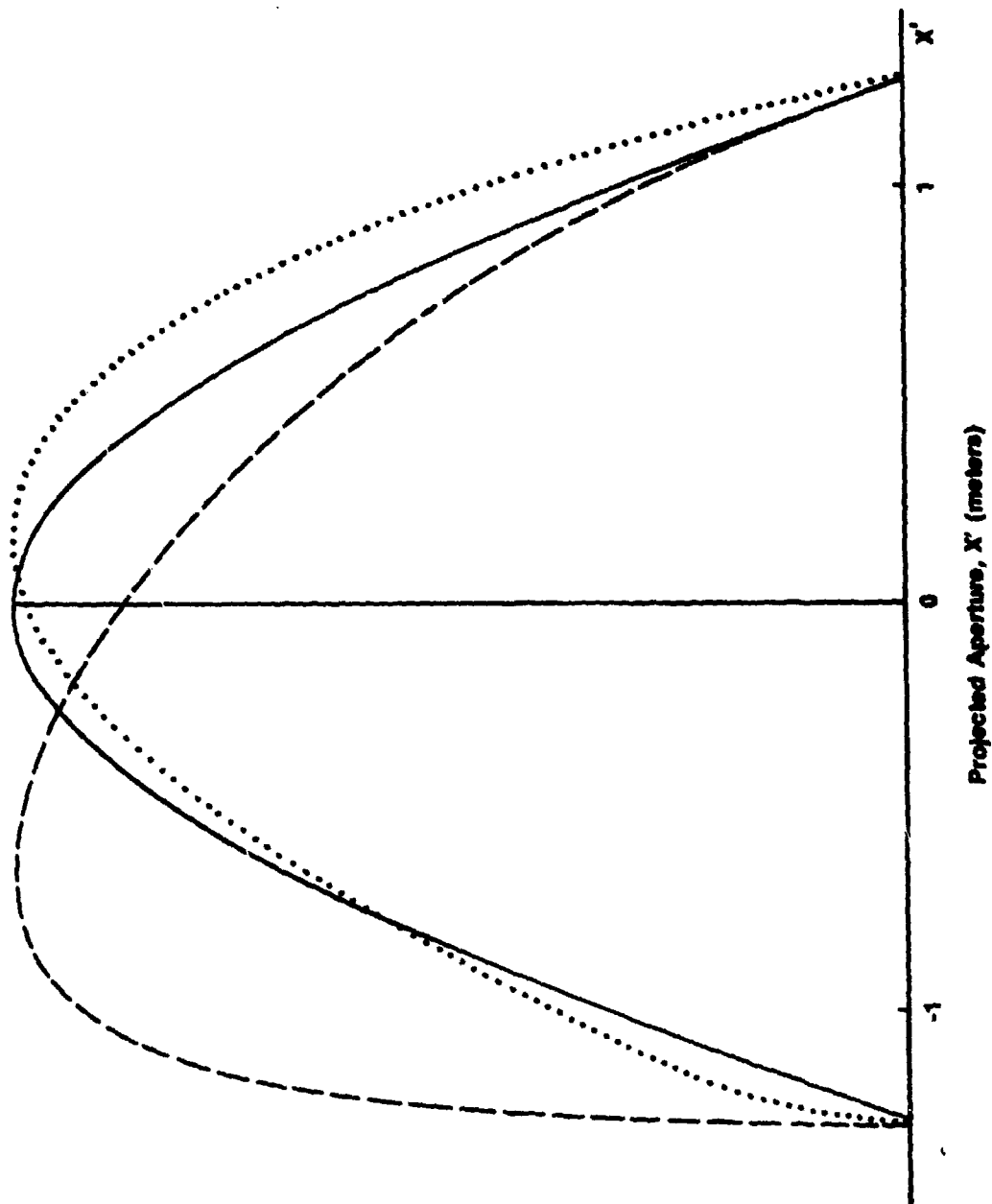
Projected Aperture, X' (meters)

Figure A2b. Amplitude at the Aperture in the Projection Plane at Scan Angle, θ_0, and Curvature, S/R. An isotropic element pattern is used. The solid line is the ideal cosine curve; the dashed line the distorted curve; the dotted line is corrected curve. $\theta_0 = 20°$, S/R = 2
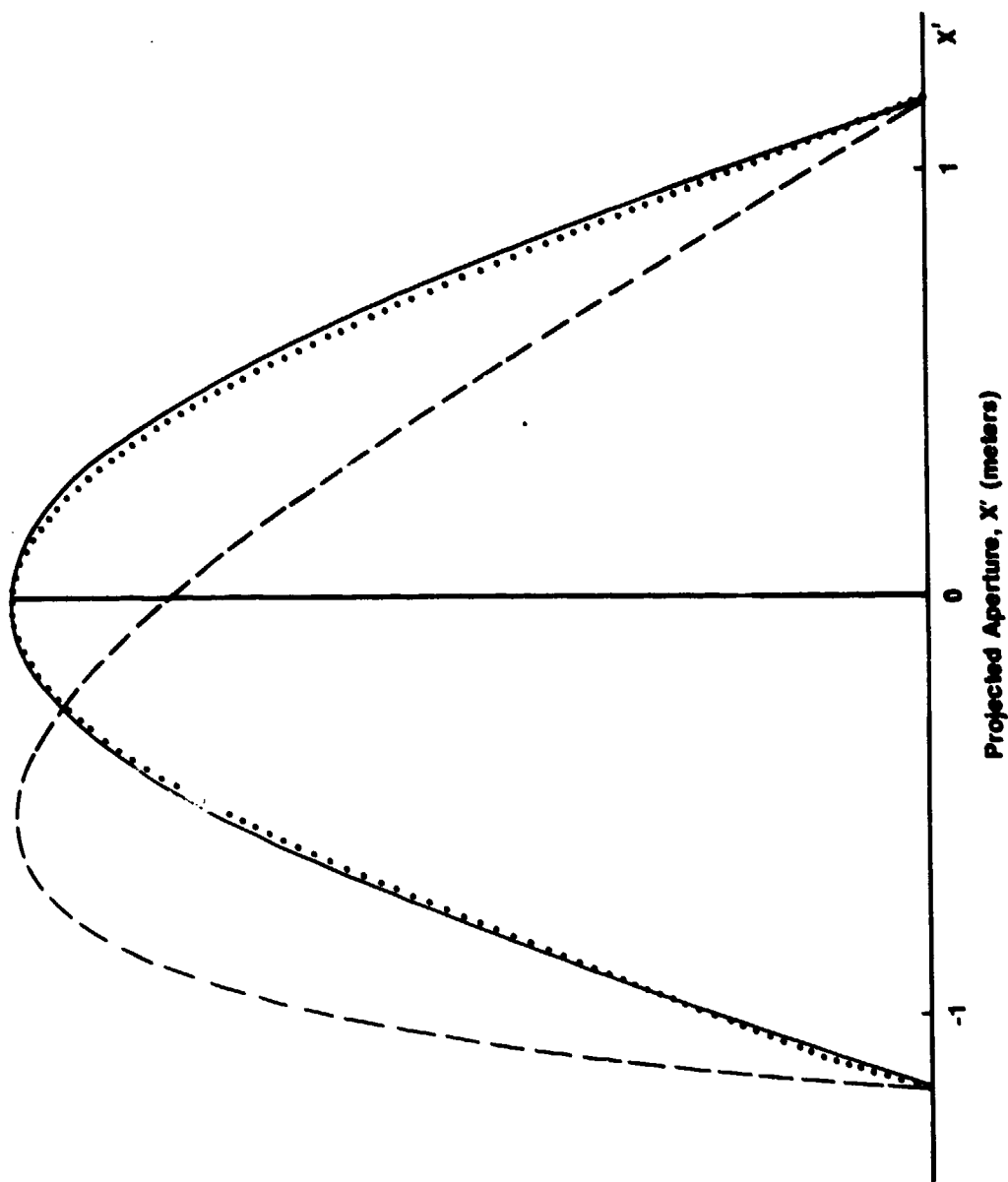
42

Figure A2c. Amplitude at the Aperture in the Projection Plane at Scan Angle, θ_0, and Curvature, S/R. An isotropic element pattern is used. The solid line is the ideal cosine curve; the dashed line the distorted curve; the dotted line is corrected curve. $\theta_0 = 40°$, $S/R = 1.07$

Figures A3a, A3b, and A3c show the radiation patterns using an isotropic element pattern. As in the previous case, the patterns are substantially improved using the correction technique. However, they have a noticeable difference; on one side of these patterns, there is a pronounced increase in the dB level of the side-lobes. This may be referred to as the curvature lobe since it comes about because of curvature. The curvature lobe starts at approximately the angle at which blockage of the elements at the other end of the array occurs. The angle, θ_B, at which the first array element is blocked is given by Eq. (16). For S/R equal to 1.07, blockage begins at 60°. As can be seen in the plots, for S/R equal to 1.07, the beginning of the curvature lobe approximately matches with θ_B. The correction factor was aimed at improving the first few sidelobes. It can be noticed that the $\cos^{1.5}(\theta)$ element pattern was able to greatly negate the curvature lobe; the apparently bunched up elements in the blocked area of the array are contributing little to the radiation field at high angles, and, therefore, do not encourage the build up of the curvature lobe. The phenomenon of the curvature lobe offers some insight into the mechanism of curvature effects.

When considering the difference pattern, it was found that the difference pattern cannot be improved when using the isotropic element pattern since the mainbeam null is minus infinity. This is because there is an equal level of power to the right of the center element as to the left of the center element. If it was necessary, the difference channel of the variable power divider could be bypassed. However, since the isotropic element pattern is not a real case the question is hypothetical.
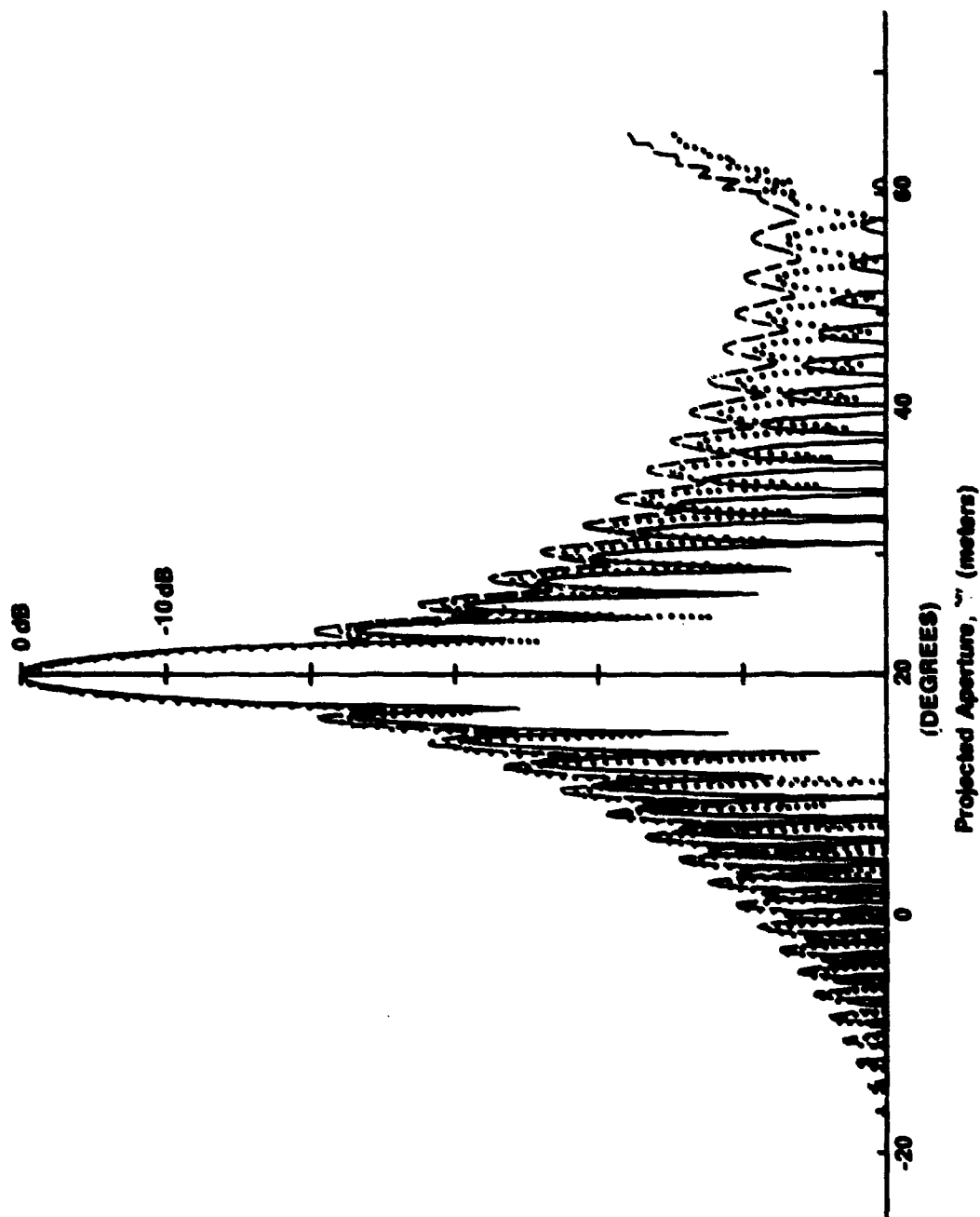
Figure A3a. Radiation Pattern Showing ± 45° Off of the Scan Angle, θ_o. An isotropic element pattern and a cosine illumination are used. The solid line is for the planar array; the dashed line is for the curved array; the dotted line is for the curved array with the correction. θ_o = 20°, S/R = 1.07

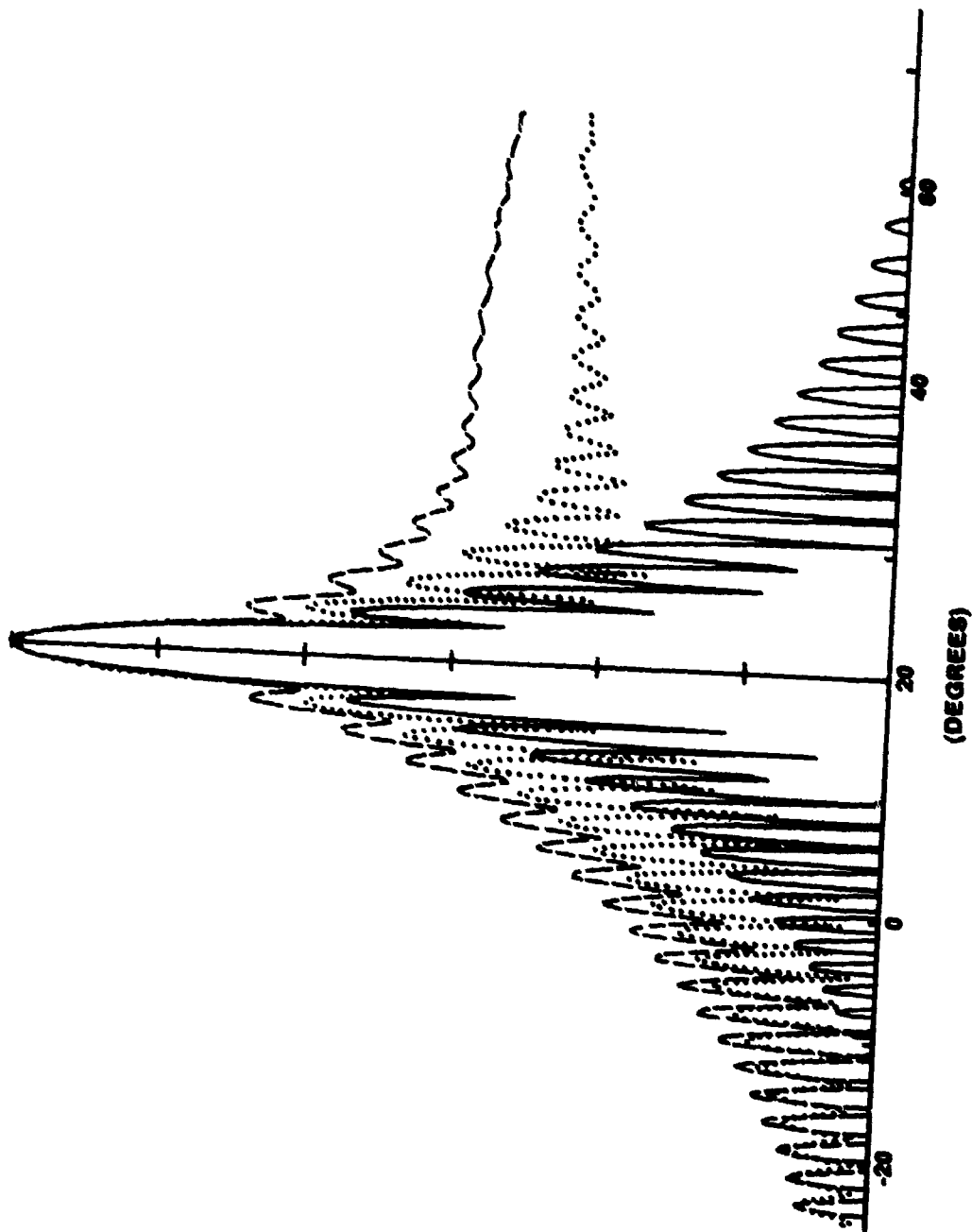*Figure A3b.* Radiation Pattern Showing ± 45° Off of the Scan Angle, θ_0. An isotropic element pattern and a cosine illumination are used. The solid line is for the planar array; the dotted line is for the curved array; the dashed line is for the curved array with the correction. $\theta_0 = 20°$, $S/R = 2$

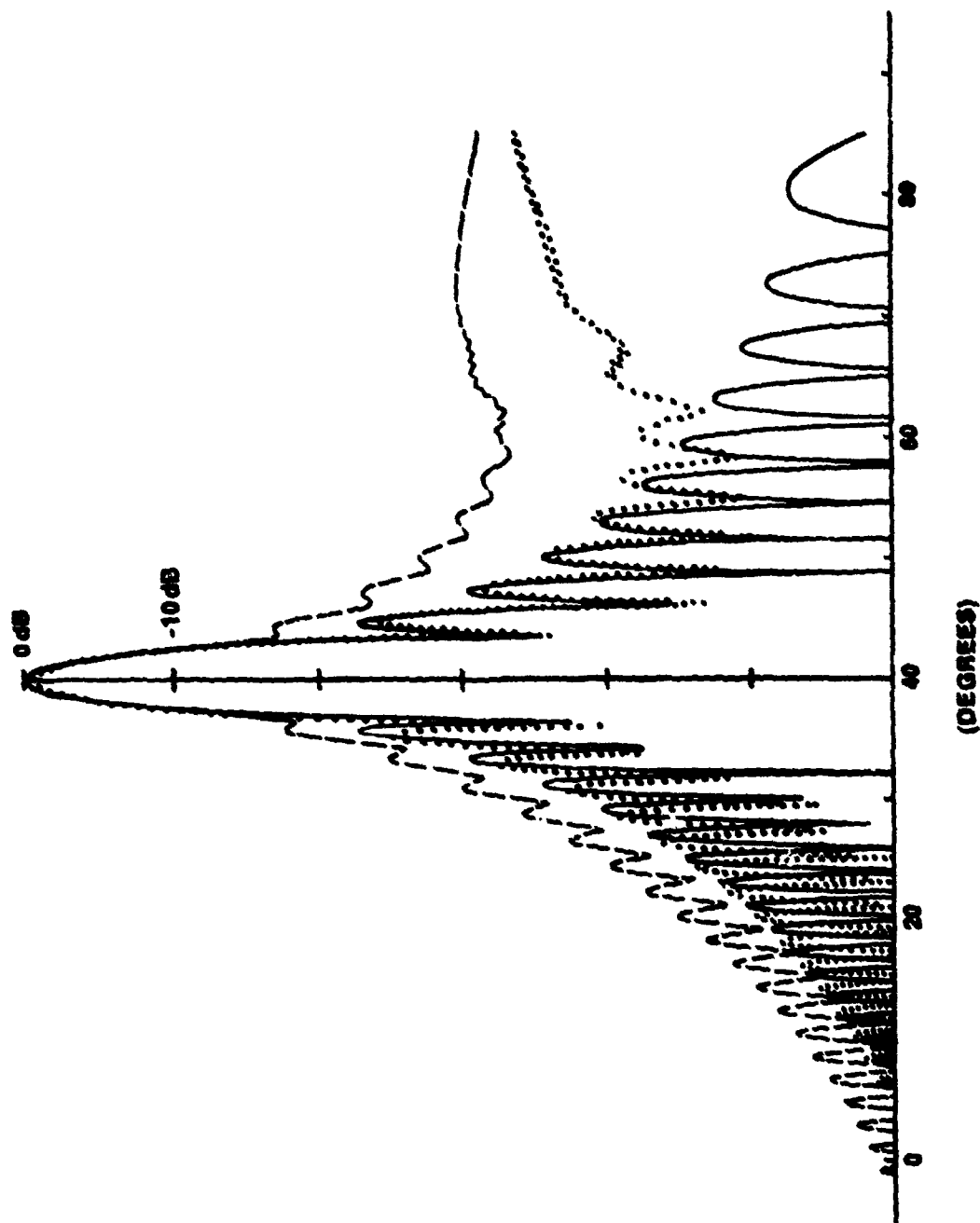(DEGREES)

Figure A3c. Radiation Pattern Showing ± 45° Off of the Scan Angle, θ_o. An isotropic element pattern and a cosine illumination are used. The solid line is for the planar array; the dashed line is for the curved array; the dotted line is for the curved array with the correction. $\theta_o = 40°$, S/R = 1.07